

# **An experimental study of two-dimensional surface water waves propagating on depth-varying currents. Part 1. Regular waves**

By **C. SWAN, I. P. CUMMINS AND R. L. JAMES**

Department of Civil & Environmental Engineering, Imperial College, London SW7 2BU, UK

(Received 14 April 1999 and in revised form 27 June 2000)

This paper describes an experimental study of two-dimensional surface water waves propagating on a depth-varying current with a non-uniform vorticity distribution. The investigation is divided into two parts. The first concerns the ‘equilibrium’ conditions in which the oscillatory wave motion and the current co-exist. Measurements of the water-surface elevation, the water-particle kinematics, and the near-bed pressure fluctuations are compared to a number of wave and wave–current solutions including a nonlinear model capable of incorporating the vertical structure of the current profile. These comparisons confirm that the near-surface vorticity leads to an important modification of the dispersion equation, and thus affects the nature of the wave-induced orbital motion over the entire water depth. However, the inclusion of vorticity-dependent terms within the dispersion equation is not sufficient to define the combined wave–current flow. The present results suggest that vorticity may lead to a significant change in the water-surface profile. If a current is positively sheared,  $dU/dz > 0$ , with negative vorticity at the water surface, as would be the case in a wind-driven current, a wave propagating in the same direction as the current will experience increased crest–trough asymmetry due to the vorticity distribution. With higher and sharper wave crests there is a corresponding increase in both the maximum water-particle accelerations and the maximum horizontal water-particle velocities. These results are consistent with previous theoretical calculations involving uniform vorticity distributions (Simmen & Saffman 1985 and Teles da Silva & Peregrine 1988).

The second part of the study addresses the ‘gradually varying’ problem in which there are changes in the current, the wavelength and the wave height due to the initial interaction between the wave and the current. These data show that there is a large and non-uniform change in the current profile that is dependent upon both the steepness of the waves and the vorticity distribution. Furthermore, comparisons between the measured wave height change and a number of solutions based on the conservation of wave action, confirm that the vorticity distribution plays a dominant role. In the absence of a conservation equation for wave action appropriate for nonlinear waves on a depth-varying current, an alternative approach based on the conservation of total energy flux, first proposed by Longuet-Higgins & Stewart (1960), is shown to be in good agreement with the measured data.

---

## 1. Introduction

Previous studies, well documented in the review articles by Peregrine (1976), Jonsson (1990) and Thomas & Klopman (1997), have shown that the interaction between a regular wave train and a steady co-flowing current is dependent upon the vertical structure of the current profile. In the simplest case involving a current which is uniform with depth (no vorticity), the wave–current interaction may be described by a simple Doppler shift (Fenton 1985). Alternatively, if the current is linearly sheared (constant vorticity) it is well known that the oscillatory wave motion remains irrotational, and that the effects of the uniform vorticity first arise as a modification to the dispersion relation. At higher orders of approximation,  $O(\varepsilon^2)$  where  $\varepsilon = ak$  is the wave steepness defined in terms of the wave amplitude  $a$  and the wavenumber  $k$ , weakly nonlinear analytical solutions (Tsao 1959; Brink-Kjaer 1976; and Kishida & Sobey 1988) show that the vorticity distribution produces changes in the water-surface elevation. This important result was further investigated in numerical calculations undertaken in deep water by Simmen & Saffman (1985) and in finite depth by Teles da Silva & Peregrine (1988). These calculations confirm that with increased nonlinearity the uniform vorticity has a profound effect upon the water-surface elevations.

Although there are many practical situations where these solutions are valid (i.e. the majority of tidal flows are approximately uniform with depth), they are not universally applicable. Indeed, if the current is generated by an external force acting on the boundary of the flow (i.e. a wind stress) a highly sheared current with non-uniform vorticity results. In this case the nonlinear wave–current interaction is dependent upon the vorticity distribution, and the oscillatory wave motion becomes rotational.

Several authors have considered the description of waves propagating on currents that vary arbitrarily with depth. For example, Kirby & Chen (1989) adopted a moderate current approximation (see Thomas & Klopman 1997) in which  $\varepsilon \ll \delta \ll 1$ , where  $\delta$  is a measure of the current strength defined by  $\delta = \tilde{U}/c$ , where  $\tilde{U}$  defines a characteristic current velocity and  $c$  is the phase velocity of the waves. Within this regime Kirby & Chen (1989) extended the deep water results of Stewart & Joy (1974) and Skop (1987) to produce a dispersion relation valid to  $O(\varepsilon\delta^2)$  for waves in finite depth. Alternatively, Swan & James (2000) considered the weak current regime,  $\delta = O(\varepsilon) \ll 1$  where the current velocity is assumed to be similar in magnitude to the first-order orbital motion, and provide a stream function solution valid to  $O(\varepsilon\delta)$ . This solution, which is particularly suited to the description of currents exhibiting strong near-surface shear, provides explicit descriptions for both the dispersion relation and the water-particle kinematics. Although these solutions provide valuable guidance as to the importance of the vorticity distribution, they are clearly limited to weakly nonlinear effects.

In contrast, the nonlinear numerical models proposed by Dalrymple (1973, 1974, 1977), Thomas (1990), Chaplin (1990) and Cummins & Swan (1993) are not similarly restricted. Although there are significant differences between these solutions, they may be sub-divided into two broad categories. The first approach is based upon the bi-linear model originally proposed by Dalrymple (1974). This divides the water column into a number of discrete layers (originally two) and approximates the current in each layer by a linear shear. This approach is not computationally intensive, and has been used to investigate a number of realistic current profiles (Dalrymple & Heidmann 1989). However, the vorticity distribution is (by definition) discontinuous, and as a result a large number of layers is required to model a strongly sheared current with non-uniform vorticity. The second approach, adopted by Thomas (1990)

and Chaplin (1990), builds upon the procedure outlined by Dalrymple (1973, 1977). These solutions are based upon the Dureuil–Jacotin transformation and involve the development of a constrained minimization problem in which the dynamic free-surface boundary condition is satisfied within a finite difference formulation. Using this approach Dalrymple (1977) considered the interaction with both a linear shear current and a current varying according to a 1/7th-power-law; while Thomas (1990) provides good agreement with a number of experimental test cases involving weakly sheared currents.

Although these solutions are well established, and have in some cases been used to provide design information, there remains an acute shortage of comparative laboratory data. Previous experimental studies have clearly acknowledged the difficulty of simultaneously generating a regular wave train and a two-dimensional steady current. If, in addition, the desired current profile has a non-uniform vorticity distribution, the problems become that much more difficult. Early studies, notably by Brevik (1980) and Brevik & Aas (1980), considered waves on an essentially uniform current. The effects of vorticity were, however, considered by Kemp & Simons (1982, 1983). In a detailed experimental study of turbulent flows over both smooth and rough beds, they considered the wave–current interaction in the near-bed region. Although these measurements provide a valuable insight into the turbulence intensity and the resulting bed stresses (with particular applications to the onset of sediment motion), a local vorticity distribution in the near-bed region does not generally affect the wave kinematics throughout the entire water column. In perhaps the most detailed investigation of vorticity effects to date, Thomas (1981, 1990) compared his numerical predictions with experimental measurements of both linear and nonlinear waves on a number of current profiles having an arbitrary distribution of vorticity. These results clearly establish the importance of vorticity in the wave–current interaction. However, the current velocities measured in the vicinity of the water surface (or just beneath the level of the wave trough) are at most weakly sheared. For example, the maximum vorticity arising close to the water surface is of order  $\omega_s = 0.12 \text{ s}^{-1}$ . Nevertheless, some important conclusions are drawn, which are discussed further in the context of the present study.

Swan (1990) presents measurements of waves on a strongly sheared current in which the vorticity distribution is approximately uniform with depth. In these cases the existing irrotational wave solutions apply. However, although these waves were not particularly steep ( $\varepsilon < 0.2$ ), comparisons with a third-order analytical model (Tsao 1959 or Kishida & Sobey 1988) are poor. In contrast, the data are in good agreement with numerical calculations provided by Chaplin (1990). These results imply that a simple measure of the wave steepness ( $\varepsilon = ak$ ) does not necessarily reflect the nonlinearity of a combined wave–current flow. Skyner & Easson (1992, 1998) also present a similar laboratory study. Although this includes some sophisticated full-field velocity measurements, their analysis of this data is based upon a time-dependent current, or one that varies with the phase of the wave cycle. This interpretation is inconsistent with the existing wave–current models, and leads to confusion regarding the segregation of the wave and the current components. This confusion, together with the use of an inappropriate irrotational wave solution (that due to Chaplin 1980), accounts for their poor description of the velocity data at certain phases of the wave cycle, notably in the vicinity of the wave trough. Klopman (1994) also provides laboratory data describing near-linear waves on both ‘favourable’ and ‘adverse’ currents. In these cases the vorticity arising at the water surface is either small or, in the case of the ‘adverse’ currents, shows little variation with depth. Nevertheless,

some interesting data concerning the wave-induced change in the current profile are provided. More recently, Groeneweg & Klopman (1998) have re-considered these data and have shown that the current change can be successfully predicted using a GLM formulation.

This paper presents the results of a new experimental study in which a series of regular waves interact with a strongly sheared current exhibiting a non-uniform vorticity distribution. These observations are appropriate to the interaction of swell waves with a wind-driven current. They may also be relevant to the description of waves at the mouth of an estuary where the intrusion of a saline wedge leads to large vertical gradients in the out-flowing current. The purpose of the present study is to investigate the influence of the vorticity distribution and to provide benchmark data against which the existing wave-current formulations can be judged. In particular, the data are compared to a five-layered numerical model based upon the bi-linear formulation originally proposed by Dalrymple (1974). This model has been investigated in a preliminary study (Cummins & Swan 1993) in which the five layers of variable depth were shown to be sufficient to model a strongly sheared current with a non-uniform vorticity distribution. Indeed, subsequent comparisons (not presented here) have shown that the results of this model are identical to those produced by the finite difference formulations proposed by Thomas (1990) and Chaplin (1990). A brief description of this model is given in the Appendix.

Section 2 commences with a description of the experimental apparatus and measuring procedure. A number of preliminary observations are also outlined. Discussion of the measured wave-current interaction is sub-divided into two sections. The first, presented in §3, describes the equilibrium conditions arising within an established wave-current combination. This concerns the interaction with both 'favourable' and 'adverse' currents, where the former corresponds to currents aligned with the direction of wave propagation and the latter to currents opposing the wave motion. Measurements of the water-surface elevation, the underlying kinematics, and the near-bed pressure fluctuations are compared with the existing irrotational solutions and the numerical model outlined in the Appendix. In contrast, §4 concerns the initial interaction between the wave and the current. This arises when a wave train first propagates onto the current, and forms part of a 'gradually varying' problem in which there are changes in the wave height, the wavelength and the current profile. These results are compared to the conservation of total energy flux first proposed by Longuet-Higgins & Stewart (1960) in their derivation of the radiation stress tensor. To further highlight the importance of the vorticity distribution these results are also compared to the fifth-order solution for waves on a uniform current (Thomas 1990), and the second-order solution for waves on a linear shear current (Jonsson, Brink-Kjaer & Thomas 1978). The practical implications of these results are discussed in §5.

## 2. Experimental work

### 2.1. Apparatus

The experimental investigation was undertaken in a purpose-built wave-current flume that has been constructed in the Department of Civil & Environmental Engineering at Imperial College. This facility is 20 m long, 0.3 m wide and has a maximum working depth of 0.7 m. The sidewalls (and two sections of the bed) are constructed from glass to provide full optical access. Smooth bed conditions are maintained throughout. The waves are generated by a flat-backed, bottom-hinged paddle located at one end of the

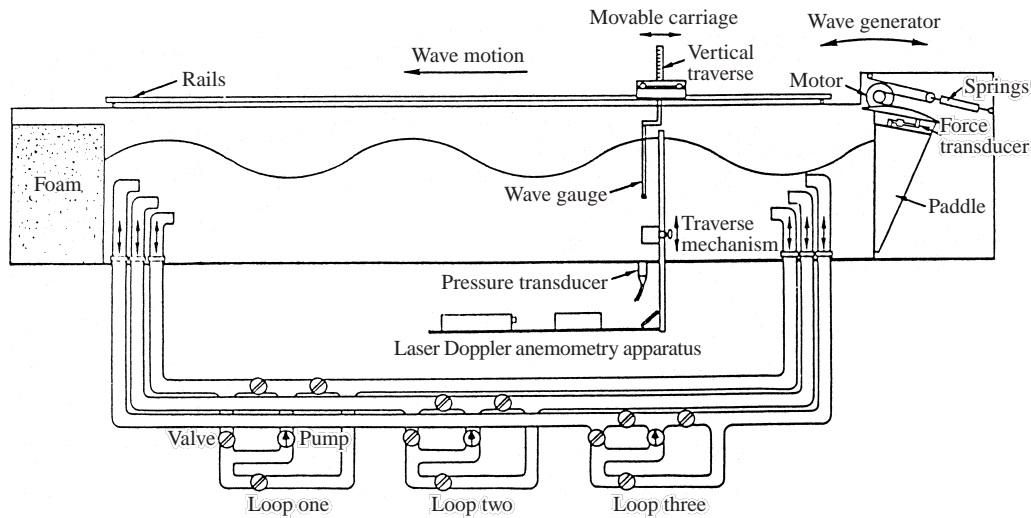


FIGURE 1. Side view of the experimental apparatus.

wave flume. The hydrostatic loads acting on the paddle are supported mechanically, via a system of springs and pulleys, and the drive system controlled numerically. This allows the successful generation of waves within a period range  $0.5 \text{ s} \leq T \leq 2.0 \text{ s}$ . At the downstream end of the flume the wave motion is absorbed by a large block of polyether foam. This is approximately 1.5 m in length where the front face has been cut to form a vertical wedge with an included angle of  $30^\circ$ . Using this method of passive absorption the largest reflection coefficient measured within the wave flume was less than 1%. Further details concerning the generation and absorption of waves within this facility are given by Baldock, Swan & Taylor (1996). The re-circulating current was introduced via three loops of 75 mm diameter pipework. Each loop is driven by a self-priming centrifugal pump, and the flow direction determined by four gate valves. This arrangement gives a variable discharge, with a total capacity of  $0.045 \text{ m}^3 \text{ s}^{-1}$ . This is sufficient to generate a uniform current of approximately  $0.2 \text{ m s}^{-1}$ , or a strongly sheared current where the near-surface velocity may be as large as  $0.6 \text{ m s}^{-1}$ . A sketch showing the layout of the experimental facility is given on figure 1.

The wave-current flume is equipped with an array of surface-piercing wave gauges. Each gauge consists of two vertical wires (1 mm in diameter) that are supported within a vertical traverse. This, in turn, is mounted on a movable carriage located on rails at the top of the wave flume. The wave gauges can thus be positioned on any vertical section, and allow the water-surface elevation to be measured with an accuracy of  $\pm 0.5 \text{ mm}$ . The underlying velocity field was measured using laser-Doppler anemometry. A 35 mW helium-neon laser was used to create a three-beam arrangement with cross-polarization. This system allows the horizontal and vertical velocity components to be measured simultaneously within a measuring volume estimated to be  $0.5 \text{ mm}^3$ . The laser beams were focused mid-way across the width of the wave flume and were positioned via a traverse mechanism that was estimated to have an accuracy of  $\pm 1 \text{ mm}$  in the vertical direction and  $\pm 2 \text{ mm}$  in the horizontal. The intersection of the laser beams was observed in a 'forward scatter' configuration using a photo-multiplier (camera) located on the opposite side of the wave flume. This approach provides the optimal signal-to-noise ratio with no disturbance of the flow field. To further improve

the signal quality the water was seeded with milk added in the ratio of approximately 10 p.p.m. After filtering to remove some high-frequency contamination, it was estimated that the velocity components could be determined to  $\pm 2\%$ . Finally, the pressure measurements discussed in §3 correspond to the output from a transducer mounted flush with the bed of the wave flume. This instrument provides a continuous record of the pressure fluctuations, and has an accuracy of  $\pm 4\%$ .

### 2.2. Inlet conditions and measuring procedure

The simultaneous generation of waves and depth-varying currents is complicated by the need to have some form of current-shaping apparatus (to produce the required velocity gradient), while at the same time allowing a mechanically generated wave train to propagate with minimal disturbance along the length of the wave flume. In the present study, two separate approaches were adopted to produce a range of sheared current profiles. In the first case, a positively sheared 'favourable' current ( $U > 0$  and  $dU/dz > 0$ , where  $U$  defines the current and  $(x, z)$  are Cartesian coordinates in which  $x$  is measured in the direction of wave propagation and  $z$  is measured vertically upwards from the bed) was produced by an up-welling flow positioned close to the wave paddle. To achieve this the outlet pipes at the upstream end of the wave flume were positioned close to the bed, and surrounded by a thick layer of polyether foam (figure 2*a*). This arrangement produced large near-surface flows (figure 4*a*) that could be straightened (across the width of the wave flume) and smoothed with additional layers of foam and honeycomb placed approximately 1 m downstream (figure 2*a*). This arrangement was adjusted (by trial and error) until a compromise was achieved in which both the required current profile and a series of regular waves could be generated at the measuring section. To ensure that the current-generating apparatus did not unduly affect the wave train, preliminary measurements were taken in which the pumps were switched off but the apparatus indicated on figure 2(*a*) remained in place. In these cases both the water-surface elevation and the underlying kinematics were in good agreement ( $\pm 3\%$ ) with a fifth-order Stokes solution (Sobey *et al.* 1987).

Unfortunately, the simultaneous generation of a negatively sheared 'adverse' current ( $U < 0$ ,  $dU/dz < 0$ ) and a regular wave train proved more difficult. In this case the need to position the current-shaping apparatus between the passive absorber and the measuring section (figure 2*b*) produced significant wave reflections capable of disturbing the flow at the measuring section. Although the introduction of an up-welling flow, as described above, was initially employed a second approach proved more successful. In this case the outlet pipes (now at the downstream end of the wave flume) were connected to a two-dimensional nozzle that directed the flow through a horizontal slot located 10–15 cm beneath the level of the wave trough (figure 2*b*). With this arrangement only a small quantity of foam (figure 2*b*) was necessary to produce the required current profile. More importantly, this approach produced a stronger current shear thereby allowing the measuring section to be moved further upstream of the current-shaping apparatus.

In the present tests the measuring section was located 3.5 m upstream of the nozzle. At this position it was possible to generate the required test conditions for the duration of 5–6 wave cycles. During this period the regular waves co-exist with the desired current profile, and the relevant experimental data are gathered before the incident wave train is disrupted by the reflected waves travelling in the opposite direction. Figure 3(*a*) shows a typical time-history of the water-surface elevation,  $\eta(t)$ , recorded at the measuring section. For  $t < 19$  s the wave conditions are evolving towards a uniform, or near-uniform, state. This is achieved within the interval  $19 \text{ s} \leq t \leq 25 \text{ s}$

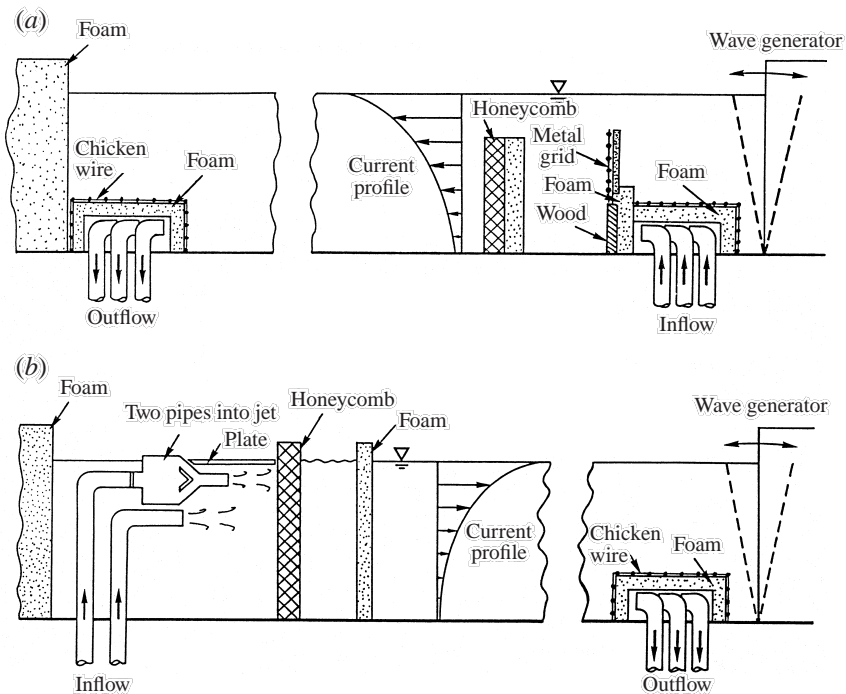


FIGURE 2. Inlet conditions: (a) generation of waves on a 'favourable' shear current; (b) generation of waves on an 'adverse' shear current.

during which the 'representative' data are recorded. For  $t > 25$  s the disturbance caused by the return of waves reflected from the downstream nozzle (figure 2b) becomes clear. The waves recorded within the sample space are reproduced at larger scale in figure 3(b). Within each of the 'adverse' current cases discussed below the largest variation in the wave height within the sample space was found to be  $\pm 2.1\%$ . A similar variation ( $\pm 2.4\%$ ) was recorded in the 'favourable' current cases. Furthermore, measurements of both the water-surface elevation and the underlying kinematics confirm that if the re-circulating current is switched off, but the current-shaping apparatus remains in place, the data collected during this sample period were again in good agreement ( $\pm 3\%$ ) with a fifth-order Stokes solution (Sobey *et al.* 1987).

In each of the test cases considered in § 3 the current profiles were weakly turbulent. For example, in a strongly sheared 'favourable' current (test case 5 on table 1) the maximum root-mean-square velocity fluctuations,  $\text{RMS}[u']$ , were less than 7% of the mean current; whilst in a typical 'adverse' current (test case 15 on table 1) this value reduces to 5%. To confidently apply a laminar flow model the turbulence effects must be overcome by averaging over an appropriately large number of wave cycles. In the 'adverse' current cases six wave cycles is clearly insufficient. To overcome this difficulty multiple runs of each test case were undertaken to ensure that the ensemble-averaged data were based on a minimum of 20 wave cycles. A similar number of wave cycles was also considered in the 'favourable' current cases.

### 2.3. Preliminary observations

It has already been noted that in the absence of a mean flow, but with the current-shaping apparatus indicated on figures 2(a) and 2(b) present, the wave motion is

Run	Wave conditions			Current profile			Comments
	Period $T$ (s)	Height $H$ (m)	Steepness $\frac{1}{2}Hk$	Surface velocity $U_s$ (m s <sup>-1</sup> )	Surface vorticity $\omega_s$ (s <sup>-1</sup> )	Depth- averaged velocity $\bar{U}$ (m s <sup>-1</sup> )	
1	0.75	0.100	0.33	—	—	—	No current, inlet fig. 2(a)
2	1.00	0.075	0.15	—	—	—	No current, inlet fig. 2(b)
3	0.75	0.083	0.22	+0.175	0	+0.171	Uniform, favourable
4	1.00	0.090	0.23	-0.190	0	-0.185	Uniform, adverse
5	0.75	0.079	0.19	+0.420	-2.09	+0.088	Favourable, constant current
6	0.90	0.083	0.15	+0.470	-1.90	+0.092	Favourable, constant current
7	1.05	0.100	0.14	+0.514	-2.21	+0.085	Favourable, constant current
8	1.20	0.106	0.13	+0.540	-2.20	+0.082	Favourable, constant current
9	1.00	0.090	0.24	-0.250	+0.58	-0.168	Adverse, constant wave
10	1.00	0.104	0.31	-0.348	+0.89	-0.153	Adverse, constant wave
11	1.00	0.111	0.34	-0.368	+1.20	-0.163	Adverse, constant wave
12	1.00	0.111	0.43	-0.540	+2.21	-0.173	Adverse, constant wave
13	0.90	0.086	0.33	-0.302	+0.87	-0.160	Adverse, constant current
14	1.00	0.094	0.28	-0.300	+0.71	-0.163	Adverse, constant current
15	1.10	0.096	0.23	-0.302	+1.03	-0.162	Adverse, constant current

TABLE 1. Equilibrium wave-current test conditions. (All test cases were undertaken in a water depth of  $d = 0.7$  m.)

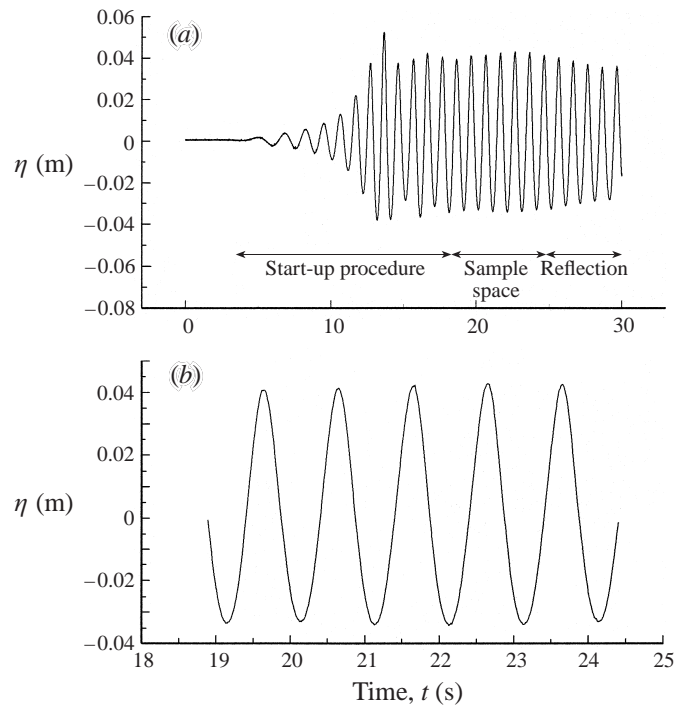


FIGURE 3. Water surface elevations,  $\eta(t)$ , recorded on a strongly sheared 'adverse' current: (a) long-term evolution ( $0 \leq t \leq 30$  s) showing initial start-up, sample space and the arrival of unwanted reflections; (b) close-up of sample space ( $19 \text{ s} \leq t \leq 24$  s).

in good agreement with existing irrotational solutions. Further preliminary measurements sought to define the characteristics of the current profile. Figure 4(a) concerns the variation in a current profile with time at one vertical section, while figure 4(b) concerns the variation across the width of the wave flume. These results, which are typical of each current profile, suggest the mean velocity is both steady and two-dimensional. Unfortunately, the uniformity of the current profile along the length of the wave flume is more difficult to maintain since both the turbulent shear stresses,  $-\overline{\rho u'v'}$ , and to a lesser extent the viscosity of the fluid, will act to reduce the magnitude of the current shear. Figure 4(c) shows the current profile measured at four vertical sections along the length of the wave flume ( $x = 0, 1.4, 2.8$  and  $4.2$  m), where  $x = 0$  is located approximately 1.5 m downstream of the honeycomb indicated on figure 2(a). Although the downstream changes in the current profile are not insignificant, the gradient in the  $z$ -direction is approximately two orders of magnitude larger than that occurring in the  $x$ -direction. For example, in the 'favourable' current cases the largest horizontal gradient was found to be  $\partial U/\partial x = -0.04 \text{ s}^{-1}$ , whilst the corresponding vertical gradient was  $\partial U/\partial z = -2.20 \text{ s}^{-1}$ . Similar values were also recorded in the 'adverse' current cases with maximum values of  $\partial U/\partial x = 0.03 \text{ s}^{-1}$  and corresponding values of  $\partial U/\partial z = 2.21 \text{ s}^{-1}$ . These values correspond to current profiles measured in the presence of waves. In the absence of waves the dominance of the vertical shear is further increased. As a result, the authors believe that a quasi-steady wave-current combination can be achieved, in which the characteristics of the wave-current interaction are primarily dependent upon the vertical shear in the current profile.

Other preliminary measurements concerned the start-up characteristics of the wave

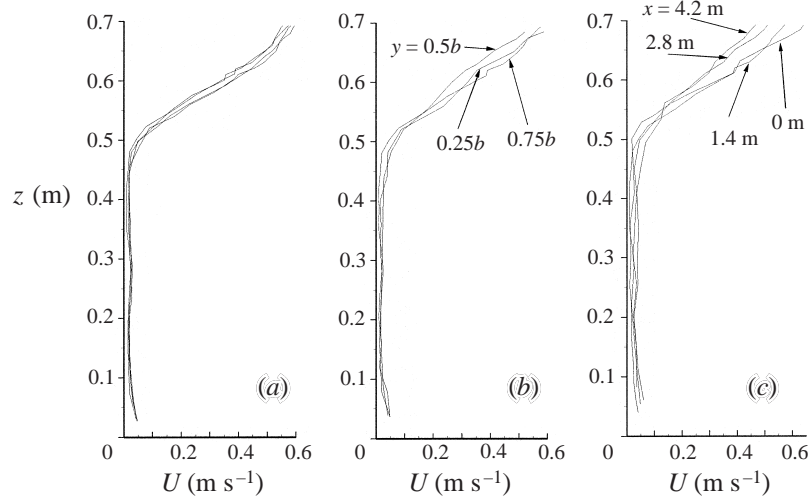


FIGURE 4. Measurements of a 'favourable' current profile,  $U$ . (a) Time variation,  $U(t)$ ; (b) cross-tank variation,  $U(y)$ , where  $y$  is measured from the sidewall and  $b$  is the flume width; (c) downstream variation,  $U(x)$ .

flume. To limit the formation of longitudinal seiching, associated with the onset of either current or wave generation, two additional precautions were adopted. First, when the re-circulating current was initially switched on the tank was allowed to settle for a period of at least 60 min. Secondly, the initial motion of the wave paddle was increased linearly from rest over a period of 2 s. This latter precaution allows the rapid generation of a regular wave train, necessary for the measuring procedure outlined above, but prevents any sudden movements of the wave paddle. Repeated measurements suggest that after applying these procedures the maximum amplitude of any longitudinal seiching was always less than 0.5 mm. Finally, the generation of a strongly sheared near-surface current often led to the formation of surface ripples. This disturbance was particularly apparent during the generation of positively sheared 'favourable' currents, since in these cases neither the honeycomb nor the foam was located at the water surface (figure 2a). However, with teepol added in the ratio of approximately 10 p.p.m. the maximum ripple height was reduced to less than 3% of the mechanically generated wave height.

### 3. Equilibrium conditions

#### 3.1. Interpretation of data

The interpretation of velocity data gathered in a combined wave-current environment is complicated by the definition of the current profile. In a fundamental sense Thomas & Klopman (1997) define a current as that part of the mean flow which does not depend upon the presence of the wave field for its existence. In a laboratory study the laser-Doppler anemometer, described previously, provides a time-history of the velocity at one point fixed in space. The simplest and most common approach is thus to define the mean velocity by time-averaging the Eulerian velocity data over a large number of complete wave periods. There are two difficulties associated with this approach. First, the mean velocity will include an element of the flow associated with the waves and does not therefore strictly correspond to the current velocity. Secondly, and more importantly, the intermittence of the velocity data above the level of the

wave trough (i.e. within the trough to crest region) precludes the determination of a meaningful mean velocity. As a result, even if the first difficulty is neglected, neither the surface current nor the near-surface vorticity distribution can be assessed using this approach. Alternatively, the laboratory data may be interpreted within a steady frame of reference in which the wave is brought to rest. Within this steady frame the mean velocity may be calculated along an empirically determined streamline rather than at one point fixed in space. This approach, which has been widely applied in the study of air flows over a curved boundary (Hsu, Hsu & Street 1981), removes the difficulty of defining the current profile and thus the vorticity distribution in the vicinity of the water surface.

Although the benefits of this latter approach are significant, it also introduces some uncertainty because the calculation of an average velocity along an empirically determined streamline provides a Lagrangian description of the mean flow. As a result, the calculated average will incorporate the wave-induced Stokes drift. Since this component of the mean flow arises as a consequence of the wave motion, it should not be considered as part of the current that interacts with the wave motion. At a second order of wave steepness, the additional Lagrangian drift in irrotational waves (in the absence of a current) is defined by

$$\bar{U}_{Stokes} = \frac{a^2 k \sigma \cosh(2kz)}{2 \sinh^2(kd)}, \quad (1)$$

where  $a$  is the wave amplitude,  $k$  the wavenumber,  $\sigma$  the wave frequency,  $d$  the water depth and  $z$  is measured vertically upwards from the bed. At this point it is perhaps important to note that no attempt has been made to introduce the additional Eulerian back-flow necessary to ensure that the net wave-induced mass flux across any vertical section is zero. As a result, the present calculations are based upon Stokes first definition of the phase velocity in which the wave motion, at any fixed point always below the water surface, has a zero Eulerian average. Further consideration of this point is given in §3.2. More importantly, higher-order irrotational calculations (Swan & Sleath 1990) confirm that (1) provides a reasonable description of the wave-induced drift in the absence of a current. Nevertheless, it is only accurate to a second order of wave steepness,  $O(\varepsilon^2)$ , and does not incorporate the effect of the viscous boundary layers occurring at either the free surface or the bed. In this latter respect, the so-called ‘conduction solution’ proposed by Longuet-Higgins (1953) may be applicable. However, this solution requires the development of a fully diffused vorticity profile. Given the magnitude of the turbulent fluctuations, discussed below, this would take many wave cycles to evolve (see also Swan 1990) and is therefore inappropriate.

More significantly, Dingemans (1997) provides a useful expression for the wave-induced drift that takes account of the orbital fluid motion, the displacement of the fluid particles, and the vertical structure of the mean flow. This solution is appropriate to the description of rotational waves on currents with depth-varying vorticity. However, for the wave-current combinations considered in the present study, calculations based on this approach show only small variations ( $\pm 5\%$ ) from those predicted by (1). Indeed, repeated calculations confirm that the uncertainty in the wave-induced drift is very small in comparison with the magnitude of the shear current. As a result, the current velocity is determined by averaging the measured velocity over one wavelength along an empirically determined streamline (specified in a steady frame of reference), and subtracting the second-order Stokes drift defined in (1). Having undertaken this procedure the data are returned to a stationary reference

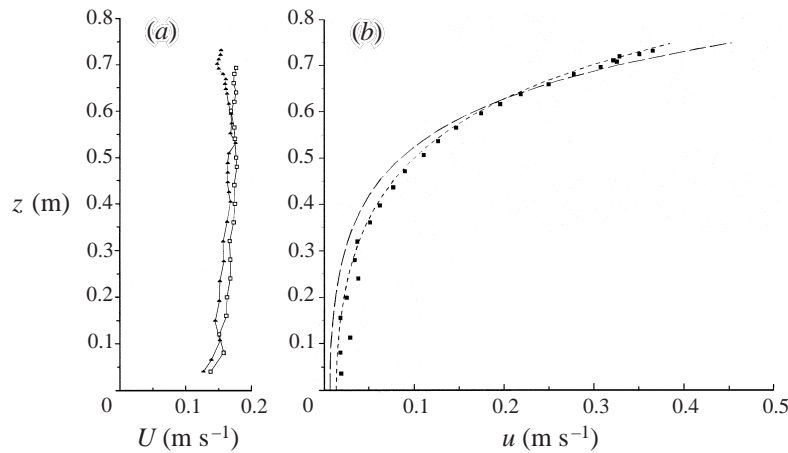


FIGURE 5. Interactions with a 'favourable' uniform current, case 3. (a) Current profile: □, initial current; ▲, current measured in presence of waves. (b) Wave kinematics: ■, horizontal velocity measured beneath wave crest; ---, waves-only solution,  $U = 0$ ; -.-.-, Doppler-shifted solution,  $U = U_s$ .

frame by adding the measured phase velocity. Using this approach it is estimated that the maximum error in the current profile determined in the presence of waves is small ( $\pm 5\%$ ). Nevertheless, this potential error is further considered with regard to the change in the current profile discussed below. More importantly, this approach provides the most effective method of defining both the current velocity and the vorticity distribution close to the water surface.

### 3.2. Waves on a uniform current

The test conditions investigated in the present study are outlined in table 1. In each case the data describe the wave conditions and the current profile in the combined wave-current flow. In terms of the current profile the data describe the surface velocity  $U_s$ , and the surface vorticity,  $\omega_s$ , where the subscript  $s$  refers to conditions at the water surface ( $z = \eta + d$ ). In addition, the depth-averaged current,  $\bar{U}$ , is also defined for each test case.

Cases 1 and 2 correspond to the preliminary (waves-only) measurements discussed in §2, whereas cases 3 and 4 respectively concern the interaction with a 'favourable' uniform current ( $U > 0$ ) and an 'adverse' uniform current ( $U < 0$ ). In these latter cases the current has no significant vorticity distribution ( $dU/dz \simeq 0$ ), and consequently the measured data are in good agreement with a simple Doppler-shifted solution. For example, figure 5(a) concerns case 3, and presents two current profiles. The first, indicated by the square symbols, shows the current profile measured in the absence of waves; while the second, indicated by the triangular symbols, represents the current measured in the presence of waves using the method outlined above. In this latter calculation the data define the current profile directly beneath a wave crest. At this phase of the wave cycle the empirically determined streamlines, along which the measured data were averaged, are displaced upwards giving rise to data located above the mean water level. In effect, the vertical axis of figure 5(a) defines the absolute position of the streamlines beneath a wave crest. This approach is adopted in all subsequent descriptions of the current profile.

The data presented on figure 5(a) suggest that in case 3 the only change in the current profile corresponds to the addition of a small back-flow having a depth-

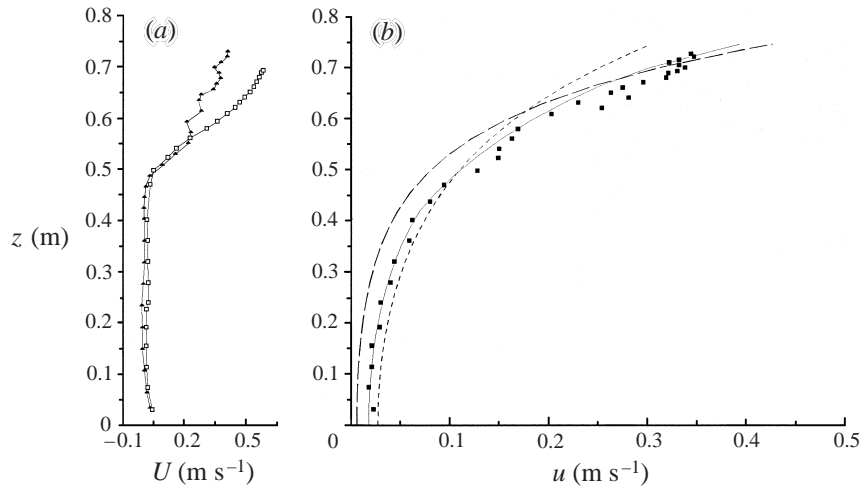


FIGURE 6. Interactions with a strongly sheared ‘favourable’ current, case 5. (a) Current profile:  $\square$ , initial current;  $\blacktriangle$ , current measured in presence of waves. (b) Wave kinematics:  $\blacksquare$ , horizontal velocity measured beneath wave crest;  $---$ , waves-only solution,  $U = 0$ ;  $\cdots$ , Doppler-shifted solution,  $U = U_s$ ;  $—$ , multi-layered numerical model,  $U = U(z)$ .

averaged value of  $\Delta U = -11.2 \text{ mm s}^{-1}$ . Assuming that the presence of the waves does not affect the discharge of the pumps (this was subsequently confirmed by measuring the velocity profile across an outlet pipe), it seems likely that this back-flow is established in order to compensate for the Stokes drift defined in (1). Indeed, if it is assumed that this return-flow occurs uniformly with depth, a current change of  $\Delta U = -\frac{1}{2}a^2\sigma \coth(kd)/d$  is predicted. In case 3 this corresponds to  $\Delta U = -10.3 \text{ mm s}^{-1}$ , which is very close to the measured value given above. This result is typical of the interaction with both ‘favourable’ and ‘adverse’ uniform currents (cases 3 and 4), but is in marked contrast to the interaction with sheared currents (cases 5–15) discussed below.

Figure 5(b) again concerns case 3 and compares the horizontal component of the wave-induced orbital velocity,  $u(z)$ , measured beneath a wave crest, with both a fifth-order Stokes solution and the fifth-order Doppler-shifted solution proposed by Fenton (1985). In this, and many subsequent comparisons, the Stokes solution neglects the current and provides a waves-only solution, while the Doppler-shifted solution assumes the current is constant with depth and defined by  $U = U_s$ , where  $U_s$  is the current velocity at the water surface. In both case 3 (figure 5b) and case 4, the Doppler-shifted solution provides a good description of the measured data. If the numerical model outlined in the Appendix is applied to these cases the predicted kinematics are identical to the Doppler-shifted solutions.

### 3.3. Waves on a sheared current

#### 3.3.1. Changes in the current profile

A similar sequence of results concerning the interactions with a positively sheared ( $dU/dz > 0$ ) ‘favourable’ current ( $U > 0$ ) is presented on figures 6, 7 and 8. These correspond to cases 5, 6 and 7 outlined in table 1, and consider the interaction of three distinct wave trains ( $T = 0.75, 0.90$  and  $1.05 \text{ s}$ ) with the same undisturbed current profile. In contrast, figures 9, 10 and 11 concern cases 10, 11 and 15 (table 1), in which the current is ‘adverse’ ( $U < 0$ ) and negatively sheared ( $dU/dz < 0$ ), although the

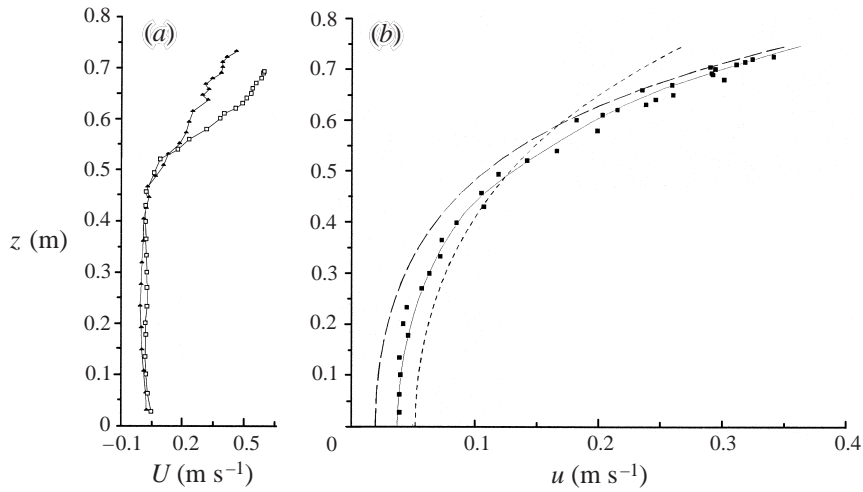


FIGURE 7. As figure 6 but for case 6.

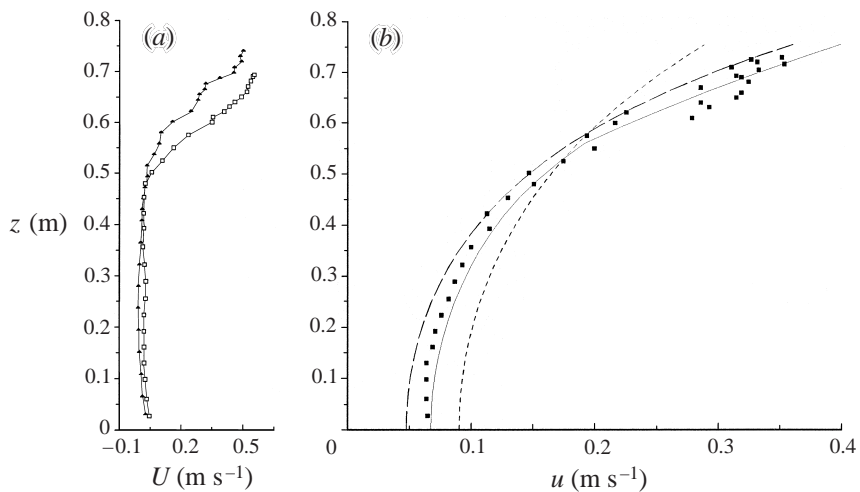


FIGURE 8. As figure 6 but for case 7.

magnitude of the vorticity arising at the water surface is less than that observed in the ‘favourable’ current examples, cases 5–7. Unlike the previous uniform current case (figure 5*a*) the data presented on figures 6(*a*), 7(*a*), 8(*a*) and 9(*a*), 10(*a*), 11(*a*), suggest that the wave–current interaction produces a significant and non-uniform change in the current profile. In each of these cases, and indeed all the cases indicated in table 1, there is clear evidence of a small additional back-flow in the lower half of the flow field. This is similar in magnitude to that observed in figure 5(*a*) and again represents the return-flow necessary to balance the Stokes drift. However, a much larger change in the current is observed close to the water surface, where both the amplitude of the wave-induced orbital motion and the shear in the current profile are a maximum.

In the ‘favourable’ current cases, figures 6(*a*), 7(*a*) and 8(*a*), the wave motion produces a reduction in the magnitude of both the near-surface current and the vorticity distribution. At first sight these results perhaps suggest that the current change may be explained by additional wave-induced mixing. Indeed, previous studies

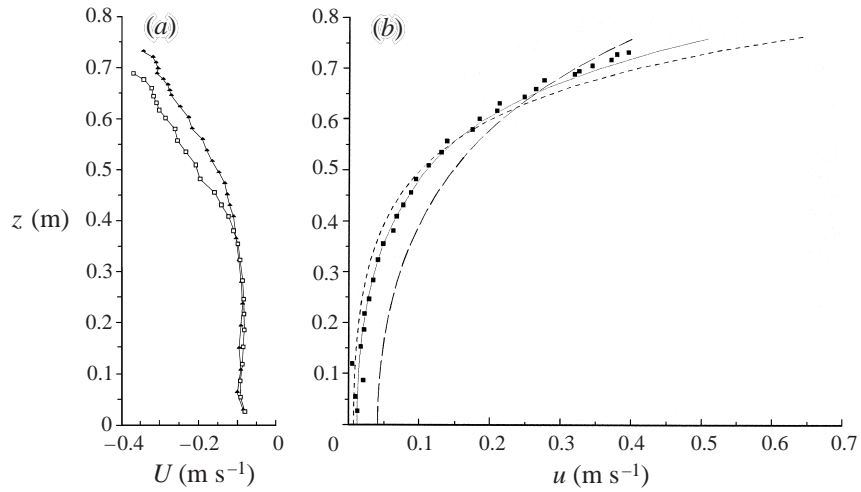


FIGURE 9. Interactions with a strongly sheared 'adverse' current, case 10. (a) Current profile:  $\square$ , initial current;  $\blacktriangle$ , current measured in presence of waves. (b) Wave kinematics:  $\blacksquare$ , horizontal velocity measured beneath wave crest;  $---$ , waves-only solution,  $U=0$ ;  $\cdots$ , Doppler-shifted solution,  $U=U_s$ ;  $—$ , multi-layered numerical model,  $U=U(z)$ .

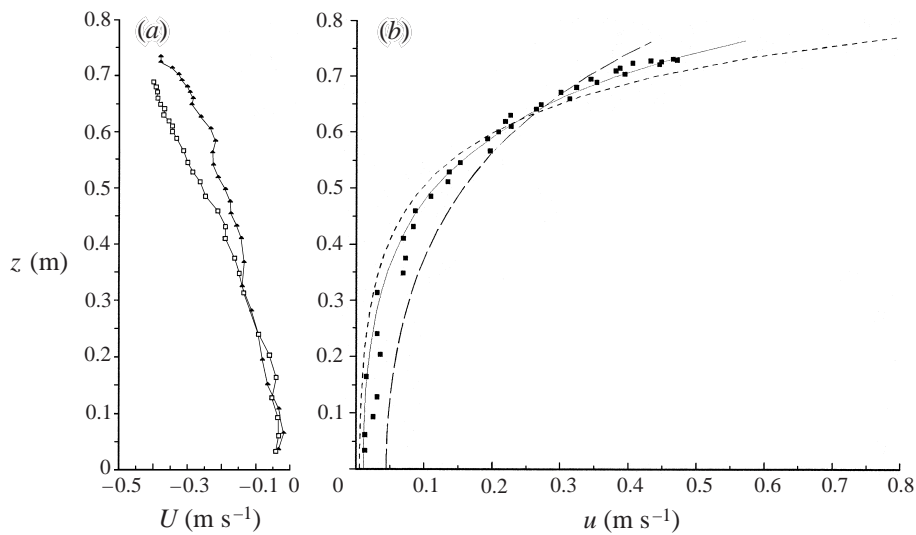


FIGURE 10. As figure 9 but for case 11.

concerning the dilution of a jet discharged in waves (Koole & Swan 1994) have shown that this effect can be significant. However, in the 'adverse' cases the current change is markedly different. In cases 10, 11 and 15 on figures 9(a), 10(a) and 11(a) there is little or no change in the magnitude of the surface current and some evidence that the near-surface vorticity actually increases. Indeed, in several other cases the interaction with the wave motion leads to significant increases in both the magnitude of the near-surface velocity and the vorticity. Figure 12(a) (corresponding to case 12) provides the best example of this effect. To highlight the contrast between the 'favourable' ( $U > 0$ ) and the 'adverse' ( $U < 0$ ) current cases, data describing the current changes

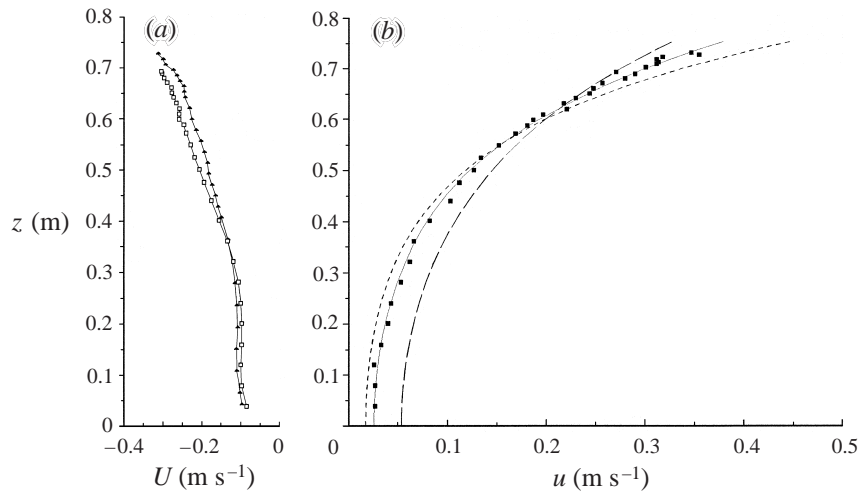


FIGURE 11. As figure 9 but for case 15.

recorded in case 5 are also presented. These comparisons clearly suggest that the current change cannot be explained by a simple increase in the vertical mixing.

The nature of the current change observed in the present tests is in broad agreement with the laboratory results presented by Klopman (1994), although the magnitude is considerably larger since the current is more strongly sheared. The effect of the current shear ( $dU/dz$ ) is examined in figure 12(b). This concerns cases 9–12, which involve an identical wave train ( $T = 1.0$  s) interacting with four different current profiles. In these cases the magnitude of the surface current change,  $\Delta U_s$ , is shown to be dependent upon the near-surface vorticity,  $\omega_s$ . However, other test cases also suggest that  $\Delta U_s$  is strongly dependent upon the steepness of the incident waves,  $ak$ , where both  $a$  and  $k$  are determined from the measured data. For example, figure 12(c) concerns cases 5–8 involving four wave trains, of differing steepness, interacting with the same undisturbed current. These data show that  $\Delta U_s$  is dependent upon the steepness of the incident wave train rather than the amplitude of the orbital motion. For example, case 5 corresponds to the steepest incident wave train ( $\varepsilon = 0.28$ ) and produces the largest current change ( $\Delta U_s = -0.16 \text{ m s}^{-1}$ ), despite the fact that it has the smallest wave height and therefore also the smallest particle orbits.

In other respects the amplitude of the wave-induced orbital motion is clearly significant. Contrasting cases 5 and 7 on figures 6(a) and 8(a), confirms that the vertical extent of the current change is strongly wave dependent. Case 5 is effectively a high-frequency wave in which the amplitude of the orbital motion decays rapidly with depth, while case 7 represents a longer wave with reduced depth decay. Although both wave cases generate maximum horizontal velocities of  $u \simeq 0.4 \text{ m s}^{-1}$  at the water surface, 0.3 m below the still water level ( $z = 0.4 \text{ m}$ ) the velocity generated by wave case 5 is less than half that associated with wave case 7. As a result, the modification of the current profile observed in case 7 extends to almost twice the depth of that recorded in case 5. The significance of this current change,  $\Delta U(z)$ , in terms of the initial wave–current interaction is considered in § 4.

### 3.3.2. Wave kinematics

Figures 6(b), 7(b), 8(b) and 9(b), 10(b), 11(b), again concern the ‘favourable’ cases 5, 6, 7 and the ‘adverse’ cases 10, 11, 15. In each of these examples measured data

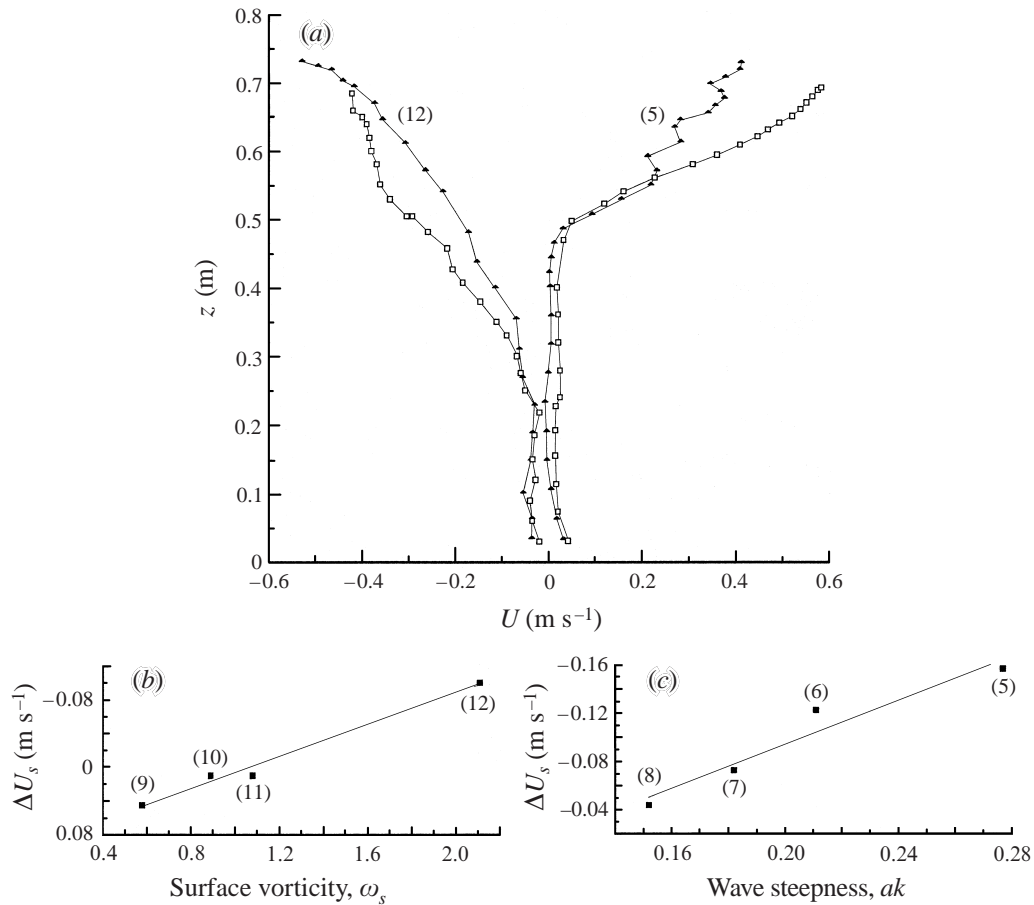


FIGURE 12. Changes in the current profile. (a)  $U(z)$ , cases 5 and 12:  $\square$ , initial current;  $\blacktriangle$ , current measured in presence of waves. (b) Current change,  $\Delta U_s$ , vs. surface vorticity,  $\omega_s$ . (c) Current change,  $\Delta U_s$ , vs. wave steepness,  $ak$ . Number in brackets refers to case.

describing the horizontal component of the wave-induced velocity,  $u(z)$ , in phase with the wave crest is compared with three possible solutions. The first represents a fifth order waves-only solution (Sobey *et al.* 1987) which neglects the effects of the current profile, i.e.  $U = 0$ . The second provides a Doppler-shifted solution (Fenton 1985) based upon the current velocity arising at the water surface, i.e.  $U = U_s$ . This solution correctly models the Doppler shift, to a fifth order of approximation, but neglects the vorticity distribution associated with the vertical structure of the current. In contrast, the third solution defines the results of the numerical model outlined in the Appendix, and thus incorporates the magnitude of the surface current,  $U_s$ , and its vertical structure,  $U(z)$ . In each case the measured data are shown to be in good agreement with the numerical model throughout the water depth. However, to achieve this level of agreement the wave-current interaction must be based on the current profile measured in the presence of the waves.

The laboratory data presented in figures 6(b), 7(b) and 8(b) also confirm that although the 'favourable' current profiles are such that significant current velocities only occur in the upper fluid layers ( $z > 0.4$ ), the wave-current interaction alters the oscillatory motion over the entire water depth. This arises because the dispersion equation (relating the wavenumber, the wave frequency and the water depth) depends

strongly on the nonlinear boundary conditions evaluated at the free surface,  $z = \eta + d$ . Thus the wavenumber, which essentially determines the decay of the oscillatory motion with depth, has a strong dependence on the near-surface values of the current and the vorticity. Considering first the oscillatory motion in the lower half of the flow field ( $z < 0.35$ ), the measured data are in good agreement with the numerical model, and lie between the waves-only and the Doppler-shifted solution. Given that the wave-current interaction within this regime is dominated by the modification of the dispersion equation, the present results are qualitatively consistent with recent analytical work in which the effect of the vorticity distribution was shown to counteract the Doppler shift based on the surface current. Swan & James (2000) give the modified dispersion equation appropriate to waves on a strongly sheared current as

$$c = \left[ \frac{g}{k} \tanh kd \right]^{1/2} + U_s - \frac{U'_s}{2k} \tanh kd + \frac{U''_s}{4k^2} - \frac{U'''_s}{8k^3} \tanh kd - \frac{Q}{2} \operatorname{sech}^2 kd, \quad (2)$$

where the prime denotes a vertical derivative evaluated at the water surface, and  $Q$  is a constant for a given wave-current interaction.

Equation (2) arises from a weakly nonlinear model in which the current is assumed weak ( $\delta = O(\varepsilon) \ll 1$ ) and the perturbation is expanded to  $O(\varepsilon\delta)$ . Given this approximation, the first three terms on the right-hand side of (2) are consistent with the findings of Tsao (1959) and Kishida & Sobey (1988). However, care must be exercised in making comparisons of this type since the latter two solutions, involving uniform vorticity, make no prior assumptions concerning the magnitude of the current. Accordingly, the  $O(\varepsilon^2)$  solution proposed by Tsao (1959) will not be consistent with the  $O(\varepsilon\delta)$  solution given in (2). Swan & James (2000) confirm that within the weak current regime (2) is identical to the  $O(\varepsilon\delta)$  solution proposed by Kirby & Chen (1989), and that for the present test cases the  $O(\varepsilon\delta^2)$  correction is small. This latter conclusion is, however, only applicable within the weak current regime. For the purpose of the present investigation it may be noted that if the current shear at the water surface,  $U'_s$ , is of the same sign as the surface velocity,  $U_s$ , the associated vorticity acts to reduce the Doppler shift and thereby limits the change in the wavenumber.

At higher elevations within the flow field the nature of the wave-current interaction is undoubtedly more complicated. Figures 6(b), 7(b), 8(b) and 9(b), 10(b), 11(b), again confirm that the measured data are in good agreement with the numerical model. However, this agreement provides little by way of physical explanation. In contrast, the uniform-vorticity solution (Tsao 1959) provides clear evidence of the development of additional irrotational velocity components due to the interaction with the current; whilst Swan & James (2000) identify rotational wave components of  $O(\varepsilon\delta)$  which increase towards the water surface. Although valid comparisons between this latter model and the present laboratory data are difficult, due to the model's limited nonlinearity, there is strong evidence to suggest that significant additional wave components (both irrotational and rotational) arise within the data and that they are modelled well by the numerical solution outlined in the Appendix. Indeed, the best evidence to this effect is seen in figure 8(b). This corresponds to the steepest current profile (measured in the presence of waves) and shows that the oscillatory near-surface velocities are significantly larger than those predicted by an irrotational waves-only solution. This result is surprising since the interaction with a 'favourable' current produces a reduction in both the wavenumber and the wave steepness. As a result, a reduction in the near-surface oscillatory velocities might be expected. Figure 8(b) suggests that this effect is more than offset by the development of additional wave components associated with the vorticity distribution.

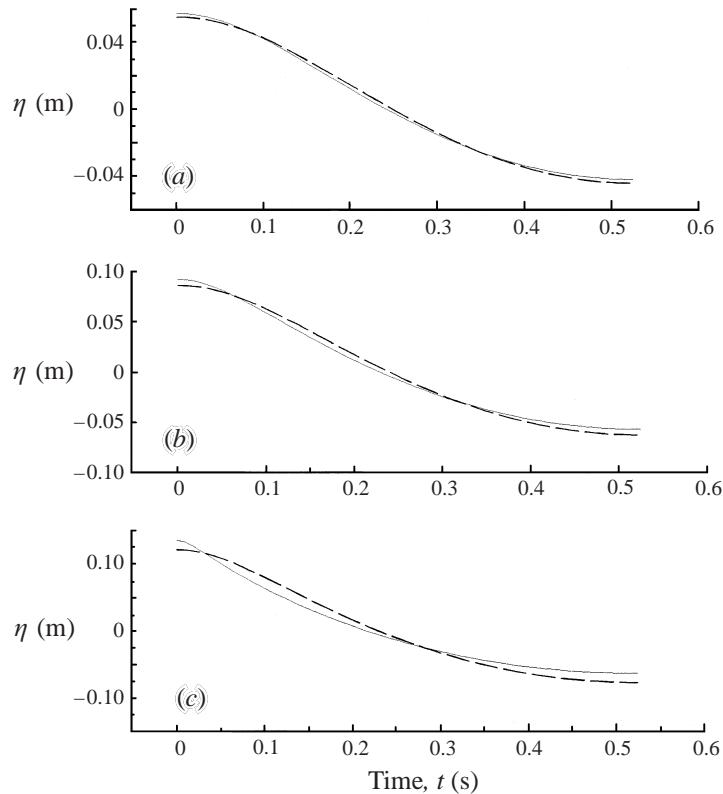


FIGURE 13. Surface elevations,  $\eta(t)$ , for waves ( $T = 1.05$  s) on current case 7. (a)  $H = 0.10$  m; (b)  $H = 0.15$  m; (c)  $H = 0.20$  m. ---, Waves-only solution,  $U = 0$ ; —, multi-layered numerical model,  $U = U(z)$ .

This result is important in two respects. First, it casts doubt on previous work (notably Hedges & Lee 1992) which has attempted to model waves on depth-varying currents in terms of an ‘equivalent’ uniform current, chosen such that the wavenumber is correctly modelled. Even if such a current could be identified, the present results suggests that the increase in the near-surface velocities could not be modelled by a simple change in the dispersion relation, the upper and lower bounds of which are given by the waves-only and Doppler-shifted solutions, respectively. Secondly, if the oscillatory velocities beneath the wave crest increase, despite a reduction in the overall wave steepness, it implies an associated change in the water-surface elevation. Tsao (1959) provides the first evidence of such a change at  $O(\epsilon^2)$  for waves on currents with uniform vorticity, whilst the numerical calculations provided by Teles da Silva & Peregrine (1988) show that the shape of extreme waves is strongly affected by a uniform vorticity distribution.

Within the present laboratory study attempts were made to investigate changes in the surface elevation due to the vorticity distribution. For the wave cases indicated in table 1 such changes lie within the measurement error described in §2 and could not therefore be rigorously identified. Attempts were also made to generate much steeper waves, but the comments of Thomas & Klopman (1997) concerning the stability of such waves proved highly relevant.

To overcome this difficulty the numerical model outlined in the Appendix was used to investigate the interaction of three wave trains with the current profile indicated

on figure 8(a). The results of these calculations are presented on figures 13(a)–13(c) and concern waves having a period of  $T = 1.05$  s and wave heights of  $H = 0.10$ ,  $0.15$  and  $0.20$  m. In each case the water-surface elevation,  $\eta(t)$ , predicted for the combined wave–current flow is compared with a nonlinear regular wave solution describing the waves acting alone, assuming both the wave height and the wave period remain unchanged. Due to the steepness of the waves involved, particularly in figure 13(c) an 18th-order stream function solution was applied. In figure 13(a) the wave conditions ( $H = 0.1$  m,  $T = 1.05$  s), which correspond exactly to test case 7 on figure 8, are such that the wave steepness calculated on the current is  $\frac{1}{2}Hk = 0.14$ , while the corresponding value for the waves-only solution is  $\frac{1}{2}Hk = 0.18$ . In this case the differences between the surface profiles are small, and appear to be consistent with the findings of Swan & James (2000). Furthermore, given the accuracy of the experimental measurements ( $\eta: \pm 1$  mm), it is clearly not possible to reliably identify changes of this magnitude. In figures 13(b) and 13(c) the wave height is increased, giving respective steepness values of  $\frac{1}{2}Hk = 0.21$  and  $0.27$  for combined waves and currents and  $\frac{1}{2}Hk = 0.26$  and  $0.33$  for a waves-only solution. In the latter case (figure 13c) the change in the water-surface elevation,  $\eta(t)$ , is considerable: the crest is higher and narrower and the trough broader and less deep. In essence, the interaction with a strongly sheared current produces a surface profile that has reduced overall steepness, measured in terms of  $\frac{1}{2}Hk$ , but increased crest–trough asymmetry.

The data presented on figure 13(c) appear consistent with the irrotational calculations for waves on a current of constant vorticity presented by Teles da Silva & Peregrine (1988). In particular, the present results should be compared to the extreme water-surface elevations shown on their figure 3, p. 289. However, the extent to which the non-uniformity of the vorticity distribution influences the magnitude of the surface elevation change, or the wave steepness at which it first becomes apparent, requires further investigation. Nevertheless, the present data confirm that the interaction between a highly nonlinear wave and a strongly sheared current with non-uniform vorticity produces two practically important effects. First, the maximum crest elevation for a given wave height is significantly increased (in the present case by 12%). Secondly, the asymmetry of the wave is such that the maximum local surface gradient ( $\partial\eta/\partial t$ ) is both increased, and arises at much higher elevations above the mean water level. These latter points have particular relevance to the calculation of the maximum water-particle acceleration and are therefore important for the determination of inertia loading.

### 3.3.3. Near-bed pressure fluctuations

The importance of the wave–current interaction is further considered in figure 14. These results concern the wave-induced pressure fluctuations recorded on the bed of the wave flume, and in both cases relate to a regular wave train ( $H = 0.101$  m,  $T = 1.2$  s and  $d = 0.7$  m) propagating on a ‘favourable’ current. In the first example, figure 14(a), the current profile was uniform with depth (current case 3 on figure 5a), while in the second, figure 14(b), the current was positively sheared (current case 5 on figure 6a). In the first example the data are compared to a fifth-order Stokes solution (Sobey *et al.* 1987) which neglects the current, and a Doppler-shifted solution (Fenton 1985). The latter solution is shown to be in good agreement with the measured data and highlights the importance of incorporating the current profile. These results confirm the strong Doppler-shift effects originally noted by Draper (1957) and discussed further by Peregrine (1976).

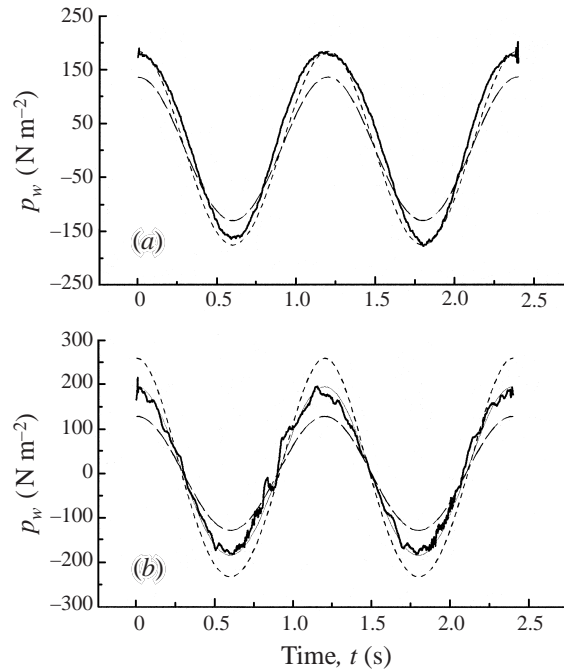


FIGURE 14. Wave-induced pressure fluctuations measured at the bed,  $p_w$ . (a) Waves on a uniform current, current case 3; (b) waves on a 'favourable' shear current, current case 5. —, Experimental data; ---, waves-only solution,  $U = 0$ ; ·····, Doppler-shifted solution,  $U = U_s$ ; ———, multi-layered numerical model,  $U = U(z)$ .

The second example (figure 14b) highlights the importance of the vorticity distribution. In this case the measured data are compared to the Stokes solution, the Doppler-shifted solution, and the results of the numerical model. In this, and several other cases involving both 'favourable' and 'adverse' sheared currents, the numerical model provides a good description of the near-bed pressure fluctuations. Indeed, these results are consistent with the previous velocity data in that the effects of the vorticity distribution are clearly significant, and act to reduce the effect of the Doppler shift. These results are of important practical significance since the pressure fluctuations measured at or near the seabed are frequently used to determine the wave conditions (for both regular and random waves) in shallow coastal waters. The present data suggest that the neglect of either the current (figure 14a) or the near-surface vorticity (figure 14b) may result in large errors in the predicted wave heights. For example, figure 14(b) suggests that errors of the order of 30% could easily arise in the predicted crest elevation if the current is strongly sheared.

#### 4. 'Gradually varying' flow

##### 4.1. Problem definition

It has already been noted that the initial interaction of waves and currents can result in a significant change in the current profile,  $\Delta U(z)$ , and that these changes must be taken into account when predicting the equilibrium conditions. In a similar manner, the wave heights used in the previous calculations were measured in the presence of the current, and have not so far been related to the wave heights generated in still water,

prior to the wave–current interaction. Indeed, the initial changes in the wavelength, the wave height and the current profile may be viewed as part of a ‘gradually varying’ flow, in which (strictly speaking) these changes take place over a scale of several wavelengths. Unfortunately, this rate of change is difficult to achieve within a laboratory wave flume where, more typically, these changes occur over a scale of one wavelength. Nevertheless, Thomas (1981, 1990) has shown that in the absence of an alternative formulation, a ‘gradually varying’ theory provides a reasonable description of nonlinear waves on a weakly sheared current. To achieve this comparison Thomas (1990) proposed a fifth-order solution based upon the conservation of wave action (Bretherton & Garrett 1968). This solution is valid for nonlinear waves on a uniform or irrotational current. However, in his figure 8 (p. 531) Thomas (1990) compares this solution with nonlinear waves on weakly sheared currents, and obtains a reasonable description of the changes in both the wavelength and the wave height. Furthermore, he concludes that the discrepancies arising within this comparison may, in part, be due to the neglect of vorticity.

To help clarify this point the present measurements are compared to both this nonlinear solution and a second-order solution for waves on a linear shear current or constant vorticity (Jonsson *et al.* 1978). This latter case has been considered more recently by Brevik & Sollie (1993, 1997) in which they calculate the fluxes of mass, momentum and energy and provide an expression for the wave energy. However, neither the  $O(\varepsilon^2)$  solution for constant vorticity or the  $O(\varepsilon^5)$  solution for waves on a uniform current (Thomas 1990) is directly applicable to the present measurements since the waves are nonlinear, and the vorticity varies strongly with depth. In an attempt to bridge this gap the authors have applied a simplistic approach based upon the total rate of energy transfer across a fixed vertical section. This approach was first applied by Longuet-Higgins & Stewart (1960) in their derivation of the radiation stress tensor. Although this analysis was originally applied to irrotational flow, Longuet-Higgins & Stewart (1960) indicate in a footnote (p. 574) that vorticity may be taken into account by supposing  $U$  to be dependent upon  $z$ . In the present calculations exactly this approach has been adopted, and the numerical model outlined in the Appendix used to determine the total rate of energy transfer both before and after the interaction with the measured current. If  $R_x$  defines the mean rate of energy transfer across a vertical plane ( $x = \text{constant}$ ), Longuet-Higgins & Stewart (1960) give

$$R_x = \overline{\int_0^{\eta} (p + \frac{1}{2}\rho\mathbf{u}^2 + \rho gz) u_x dz} \quad (3)$$

where  $\eta(t)$  defines the water surface,  $p$  is the pressure,  $\rho$  is the density,  $\mathbf{u}$  is the velocity vector ( $u_x, u_z$ ) which includes both the wave and the current components, (i.e.  $u_x = U + u$ ), and the overbar denotes the mean value with respect to time which is taken after performing the integration.

If (3) is applied prior to the interaction of the wave and the current, the mean rate of energy transfer is given by the linear sum of (a) that due to the waves, and (b) that due to the current (each acting in the absence of the other). In this case the former quantity is dependent upon the initial wave height,  $H_0$ , and may be determined from a nonlinear Stokes solution, while the latter quantity is dependent upon the undisturbed current profile,  $U(z)$ , measured in the absence of waves. Equating this sum to the mean rate of energy transfer arising in the combined wave–current flow, calculated using the numerical model outlined in the Appendix, yields an additional constraint. Provided the current profile in the presence of the wave is measured,

or can be predicted (Groeneweg & Klopman 1998), this approach allows the wave height change,  $\Delta H$ , to be determined. In the present study the current profile was measured both in the presence and absence of waves. As a result, the problem remains determinant, albeit in an iterative sense.

#### 4.2. Changes in the wavelength

Within the experimental study the wavelength was determined by cross-correlating the surface elevation data recorded from two wave gauges located 200 mm apart. This allows the time-lag between the signals to be determined and hence the phase velocity,  $c$ , of the waves. Since the wave period remains constant, the wavelength is readily determined from  $\lambda = cT$ . Using this approach it was estimated that the wavelength could be determined with an accuracy of  $\pm 10$  mm or  $\pm 1\%$ . The wavelengths associated with cases 5–8, involving the interaction with a ‘favourable’ current, are presented on figure 15(a); while cases 13–15, involving the interaction with an ‘adverse’ current, are presented in figure 15(b). These cases are also considered in tables 2(a) and 2(b) where additional calculations, based on an  $O(\varepsilon)$  solution for waves on a depth-uniform current and an  $O(\varepsilon^2)$  solution for waves on a constant-vorticity current (Jonsson *et al.* 1978) are presented. In the latter solution the linear shear (or uniform vorticity) is based on the value determined at the water surface,  $\omega_s$ . This approach is consistent with the so-called ‘depth of influence’ proposed by Teles da Silva & Peregrine (1988). In this analysis the linear dispersion equation for waves on a constant-vorticity current was used to define a depth of water (equation 2.11 on p. 284) which characterizes the depth of current that influences the wave properties. Similar arguments are also applied by White (1999) in his interpretation of a new current-induced phase shift (see his §8 p. 340). In the present laboratory cases the ‘depth of influence’ varies from 0.11 m (case 5) to 0.17 m (case 8). Within these layers the vorticity is relatively constant, and equal to the value at the water surface,  $\omega_s$ . Tables 2(a) and 2(b) also provide comparisons with the  $O(\varepsilon\delta)$  solution (Swan & James 2000) given in (2).

Figures 15(a) and 15(b) clearly demonstrate that the measured data are in good agreement with the results of the numerical model and differ significantly from both the  $O(\varepsilon^5)$  waves-only solution and the  $O(\varepsilon^5)$  Doppler-shifted solution. In addition table 2(a) confirms that in the ‘favourable’ current cases it is more important to model the vertical structure of the current profile rather than the additional nonlinear terms relating to a uniform-current approximation. This is, however, to be expected given that wave cases 5–8 are not exceptionally steep. Nevertheless, the agreement with the  $O(\varepsilon\delta)$  solution (Swan & James 2000) given in (2) is surprisingly good. Furthermore, the linearly sheared model (Jonsson *et al.* 1978) based on the vorticity at the water surface,  $\omega_s$ , is also reasonably effective.

In the ‘adverse’ current examples (cases 13–15) the value of the surface vorticity is less than that observed in cases 5–8, and the waves are steepened as they propagate onto the ‘adverse’ current. Consequently, the data provided in table 2(b) suggest that the nonlinearity associated with the irrotational components of the flow is dominant. Nevertheless, the affect of the vorticity distribution remains important. Evidence of this is given in the final three columns of table 2(b). Comparisons between the changes due to the nonlinearity associated with a uniform current and those associated with a second-order model for waves on a current with uniform vorticity, confirm that although the former quantity is generally larger, the latter is by no means insignificant. With increasing wave steepness, table 2(b) also highlights the expected limitations of the  $O(\varepsilon\delta)$  solution given in (2) relative to the full numerical model.

		Wave length on current, $\lambda$ (m)							
		Initial wave-length $\lambda_0$ (m)	Initial wave steepness $\frac{1}{2}H_0k$	$U = U_{(z)}$			${}^2U = U_s$		${}^3U = U_s - \omega_s z'$
Run number				Measured	Numerical model	$O(\varepsilon\delta)$ solution <sup>1</sup> (Eq. (2))	$O(\varepsilon)$	$O(\varepsilon^5)$	$O(\varepsilon^2)$
(a)	5	0.941	0.28	1.358	1.318	1.285	1.612	1.508	1.164
	6	1.313	0.21	1.765	1.736	1.709	2.127	2.026	1.603
	7	1.756	0.18	2.138	2.188	2.124	2.662	2.627	1.990
	8	2.218	0.15	2.508	2.645	2.559	3.200	3.193	2.420
(b)	13	1.316	0.18	0.820	0.844	0.678	0.587	0.771	0.740
	14	1.603	0.15	1.064	1.097	0.962	0.841	0.989	0.990
	15	1.902	0.12	1.341	1.373	1.292	1.116	1.202	1.436

TABLE 2. Measured and predicted wave lengths: (a) waves on a favourable sheared current, cases 5–8; (b) waves on an adverse sheared current, cases 13–15. (Calculations based on <sup>1</sup>Swan & James (2000), <sup>2</sup>Thomas (1990) and <sup>3</sup>Jonsson *et al.* (1978), with  $z' = z - d$ .)

		Wave height on current, $H$ (m)							
		Initial wave height $H_0$ (m)	Initial wave steepness $\frac{1}{2}H_0k$	${}^1U = U_{(z)}$			${}^2U = U_s$		${}^3U = U_s - \omega_s z'$
Run number				Measured	Numerical model	$O(\varepsilon\delta)$ solution	Linear $O(\varepsilon)$	Non-linear $O(\varepsilon^5)$	$O(\varepsilon^2)$
(a)	5	0.083	0.28	0.079	0.077	0.075	0.046	0.051	0.056
	6	0.088	0.21	0.083	0.081	0.078	0.051	0.055	0.061
	7	0.102	0.18	0.100	0.091	0.087	0.062	0.065	0.075
	8	0.107	0.15	0.106	0.096	0.090	0.068	0.071	0.083
(b)	13	0.075	0.18	0.086	0.094	0.106	0.184	0.107	0.150
	14	0.075	0.15	0.094	0.098	0.107	0.152	0.111	0.135
	15	0.075	0.12	0.096	0.098	0.106	0.137	0.113	0.113

TABLE 3. Measured and predicted wave heights: (a) waves on a favourable sheared current, cases 5–8; (b) waves on an adverse sheared current, cases 13–15. (Calculations based on <sup>1</sup>the total rate of energy transfer [Eq. (3)] and <sup>2,3</sup>the conservation of wave action using <sup>2</sup>Thomas (1990) and <sup>3</sup>Jonsson *et al.* (1978) with  $z' = z - d$ .)

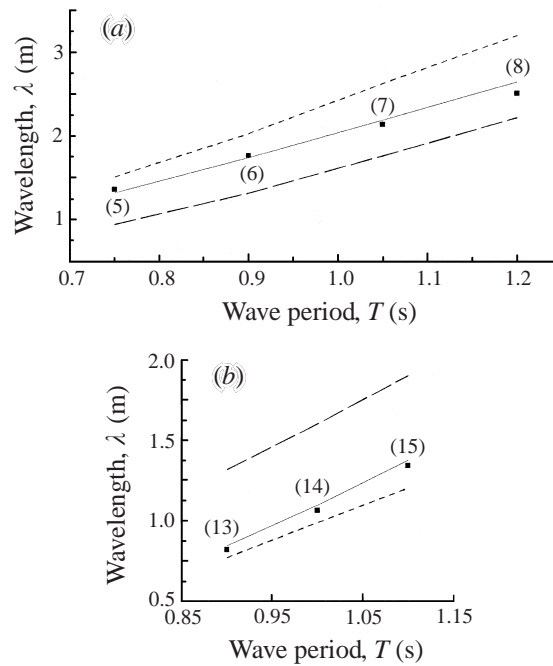


FIGURE 15. Wavelength changes. (a) Waves on a ‘favourable’ shear current, cases 5–8; (b) waves on an ‘adverse’ shear current, case 13–15. ■, Experimental data; - - - - -,  $O(\epsilon^5)$  Doppler-shifted solution,  $U = U_s$ , Thomas (1990); - · - · -,  $O(\epsilon^5)$  waves-only solution,  $U = 0$ ; —, multi-layered numerical model,  $U = U(z)$ .

### 4.3. Changes in wave height

Figures 16(a) and 16(b) again concern wave cases 5–8 and 13–15, and contrast the height of the waves after their interaction with the various currents ( $H$ ) with those recorded in the absence of the current ( $H_0$ ). The measured data are compared with four solutions, three of which are based on the conservation of wave action. The first of the three represents a linear approximation based upon a uniform current ( $U = U_s$ ) following the work of Bretherton & Garrett (1968); the second represents the fifth-order extension of this model proposed by Thomas (1990); while the third represents a second-order model appropriate to a linearly sheared current (or constant vorticity) proposed by Jonsson *et al.* (1978). Both figures 16(a) and 16(b) show that none of these solutions provides a good description of the experimental data. In contrast, the fourth solution is based upon the energy flux equation (3), with the combined wave–current motion determined using the numerical model outlined in the Appendix. This provides the only method that includes both the nonlinearity of the flow and the vertical structure of the current profile, and is shown to be in good agreement with the measured data.

Tables 3(a) and 3(b) again concern wave cases 5–8 and 13–15 and provide additional comparisons with the  $O(\epsilon\delta)$  solution proposed by Swan & James (2000). In this case the total energy flux constraint (3) has been applied, but the combined wave–current flow calculated using the  $O(\epsilon\delta)$  solution. In the ‘favourable’ current examples (cases 5–8) it is interesting to note that although the nonlinearity associated with the

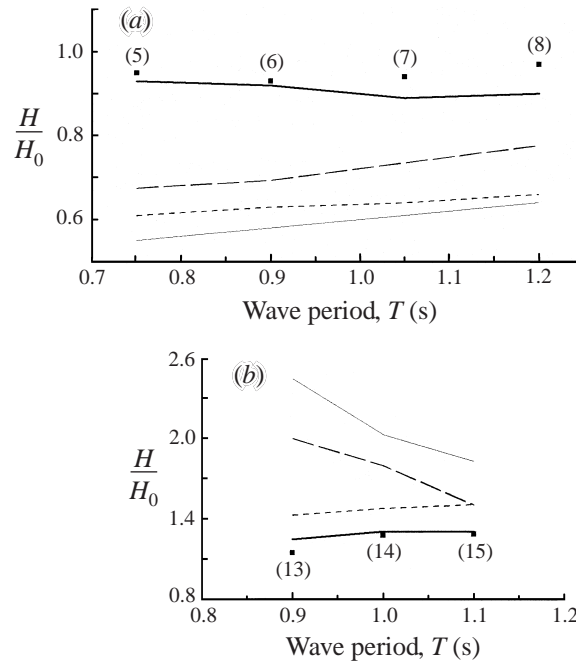


FIGURE 16. Wave height changes. (a) Waves on a 'favourable' shear current, cases 5–8; (b) waves on an 'adverse' shear current, cases 13–15. ■, Experimental data; —,  $O(\varepsilon)$  Doppler-shifted solution,  $U = U_s$ ; - - - - -,  $O(\varepsilon^5)$  Doppler-shifted solution,  $U = U_s$ , Thomas (1990); - · - · -,  $O(\varepsilon^2)$  constant vorticity solution,  $U = U_s - \Omega(z - d)$ , Jonsson *et al.* (1978); — — — —, multi-layered numerical model,  $U = U(z)$ .

irrotational flow components (i.e. a uniform-current approximation) is not particularly significant, the second-order solution based upon a linearly sheared current (constant vorticity) is in poor agreement with the measured data. In contrast, the  $O(\varepsilon\delta)$  solution provides results that are almost identical to the nonlinear numerical model. These comparisons clearly highlight the importance of the vertical structure of the current. However, in table 3(b) the increased nonlinearity of waves on 'adverse' currents (cases 13–15) again reveals the limitations of the  $O(\varepsilon\delta)$  solution.

## 5. Conclusions

The present paper has addressed the case of two-dimensional waves propagating on a vertically sheared current, in which the vorticity distribution is non-uniform. A new experimental investigation has been presented where measurements of the water-surface elevation, the water-particle kinematics, and the pressure fluctuations have been compared to a number of wave-current models. With regard to the equilibrium conditions, describing the combined wave-current motion, the existing irrotational solutions (based on a uniform-current approximation) provide a poor description of the measured data. In contrast, comparisons with a nonlinear numerical model, capable of including the vertical structure of the current profile, are good provided the interaction is based upon the current profile measured in the presence of the waves. However, the purpose of this paper is not to promote one particular model, but rather to provide the first quantitative laboratory measurements of waves on strongly sheared currents, such that the importance of the vorticity distribution can

be clearly established. In particular, it has been shown that even if the vorticity is restricted to the upper fluid layers, as would undoubtedly be the case in a wind-driven current, the inclusion of vorticity-related terms within the dispersion equation leads to a modification of the flow over the entire water depth. However, although these terms are important, it is not sufficient merely to provide an updated dispersion equation reflecting the current profile at the water surface. Indeed, in the case of a positively sheared ‘favourable’ current the present study suggests that the oscillatory water-particle velocities arising beneath a wave crest will be substantially larger than those predicted by an irrotational solution which either neglects the current or assumes that it is uniform with depth. In steep waves it is shown that the increased velocities are associated with changes in the surface profile,  $\eta(t)$ , with increased crest–trough asymmetry despite a reduction in the overall wave steepness,  $(\frac{1}{2}Hk)$ . These changes are consistent with earlier studies of waves on currents with uniform vorticity (Tsao 1959) and are closely related to the extreme wave profiles presented by Teles da Silva & Peregrine (1988).

These results are significant from a practical perspective. First, they imply that the vorticity distribution may produce increased maximum water-surface elevations for a given wave height, through increased crest–trough asymmetry. This is clearly relevant to the specification of an effective air gap necessary to prevent wave impacts on the underside of an offshore structure. Secondly, and perhaps more importantly, the data also suggest that the vorticity distribution may lead to increases in the maximum gradient of the water-surface profile,  $\partial\eta/\partial t$ . This implies larger maximum water-particle accelerations occurring at higher elevations. This result is relevant to the calculation of a wide range of inertial loads in combined waves and currents.

The paper has also considered the ‘gradually varying’ problem that arises when a wave train first propagates onto a current, with consequent changes in the wavelength, the wave height, and the current profile. The usual assumption consistent with this approach is that these changes ( $\Delta\lambda$ ,  $\Delta H$  and  $\Delta U$ ) take place over several wavelengths. However, in the present study (or, indeed, any other laboratory study) this condition is seldom upheld, with changes typically taking place over one wavelength. Despite this difficulty, Thomas (1990) obtained good agreement in a number of cases involving weakly sheared currents, but concluded that: ‘It cannot be deduced that the irrotational theory will provide a similar degree of accuracy for wave amplitude and wave length variations when the current profiles possess a greater distribution of vorticity.’ The present measurements allow the resolution of this issue, and confirm that neither the nonlinear irrotational solution proposed by Thomas (1990) nor the second-order uniform-vorticity solution proposed by Jonsson *et al.* (1978), provides a plausible description of the present data.

In the absence of a generalized conservation of wave action equation appropriate to the nonlinear interaction of waves on a general rotational current, the present study has applied the conservation of total energy flux similar to that proposed by Longuet-Higgins & Stewart (1960). Provided the current change, which is shown to be dependent on both the wave steepness and the vorticity distribution, can be determined *a priori* (in the present cases measured), the numerical model provides a good description of the changes in the wavelength, while the inclusion of the energy flux constraint allows the changes in the wave height to be accurately predicted. Similar calculations based upon the  $O(\varepsilon\delta)$  model proposed by Swan & James (2000) were also shown to be effective. Unfortunately, that model is only valid in the ‘weak’ current regime ( $\delta = O(\varepsilon) \ll 1$ ), but with no restrictions placed on the strength of the vorticity distribution. However, there appears no obvious reason why the ‘moderate’

current solutions proposed by Kirby & Chen (1989) and Thomas & Klopman (1997) should not be used in a similar manner with equal success. Indeed, the present results confirm that it is the vertical structure of the current, rather than its relative strength, that is important. Finally, it is perhaps of practical relevance to note that although the present energy flux approach requires information concerning the wave-induced current change,  $\Delta U$ , which is not typically available, the combination of this approach with recent developments reported by Groeneweg & Klopman (1998) may lead to a useful predictive tool.

This work was undertaken as part of the MAST project 'Kinematics and Dynamics of Wave-Current Interactions.' It was funded by the Commission of the European Union Directorate General for Science, Research and Development under contract no. MAS3-CT95-0011.

### Appendix. A multi-layered numerical model

The five-layered numerical model outlined in this section provides a two-dimensional representation of the equilibrium conditions arising from the interaction of waves with a depth-varying current. The proposed model is based upon the bi-linear solution originally outlined by Dalrymple (1974). In the present study the number of layers has simply been increased to provide an adequate representation of a strongly sheared current with a non-uniform vorticity distribution. If the wave motion is defined by a regular wave train propagating without change of form in a homogeneous, incompressible and inviscid fluid of constant depth, and the current is assumed to be both steady and aligned in the plane of the wave motion, a stream function,  $\psi$ , may be defined such that in a steady frame of reference:

$$(U + u - c) = -\frac{\partial\psi}{\partial z}, \quad v = \frac{\partial\psi}{\partial x}, \quad (\text{A } 1)$$

where  $(u, v)$  are the wave-induced velocity components in the  $(x, z)$ -directions,  $U$  is the steady current, and  $c$  is the phase velocity. A sketch showing both the coordinate arrangement and the solution domain is given in figure 17.

In this frame of reference the equations of motion may be simplified to give a Poisson equation:

$$\nabla^2\psi = \Omega(\psi), \quad (\text{A } 2)$$

where  $\Omega(\psi)$  defines the vorticity distribution. If the current profile is approximated by five linear segments (figure 17), the vorticity distribution is constant in each fluid layer, and the stream function,  $\psi_i$ , in the  $i$ th fluid layer ( $i = 1, 2, 3, 4, 5$ ) will be of the form

$$\psi_i = (c - U_{i-1})z - \frac{(U_i - U_{i-1})}{(d_{i-1} - d_i)} \left( \frac{z^2}{2} + d_{i-1}z \right) + \sum_{n=1}^N [X_i(n) \sinh nkz + Y_i(n) \cosh nkz] \cos nkx, \quad (\text{A } 3)$$

where  $k$  is the wavenumber,  $N$  is the order of the approximation which corresponds to the number of harmonics within the truncated series solution, and  $(U_i, d_i)$  defines the current profile (figure 17) such that  $U_0 = U_B$ , the current velocity just above the bed, and  $U_5 = U_s$ , the current velocity at the water surface. In this form the velocity potential in each fluid layer provides an exact solution to the governing field equation (A 2).

If, in a typical wave-current interaction, the current profile  $(U_i, d_i)$  is specified together with the wave height,  $H$ , and the wave period,  $T$ , of the co-existing wave

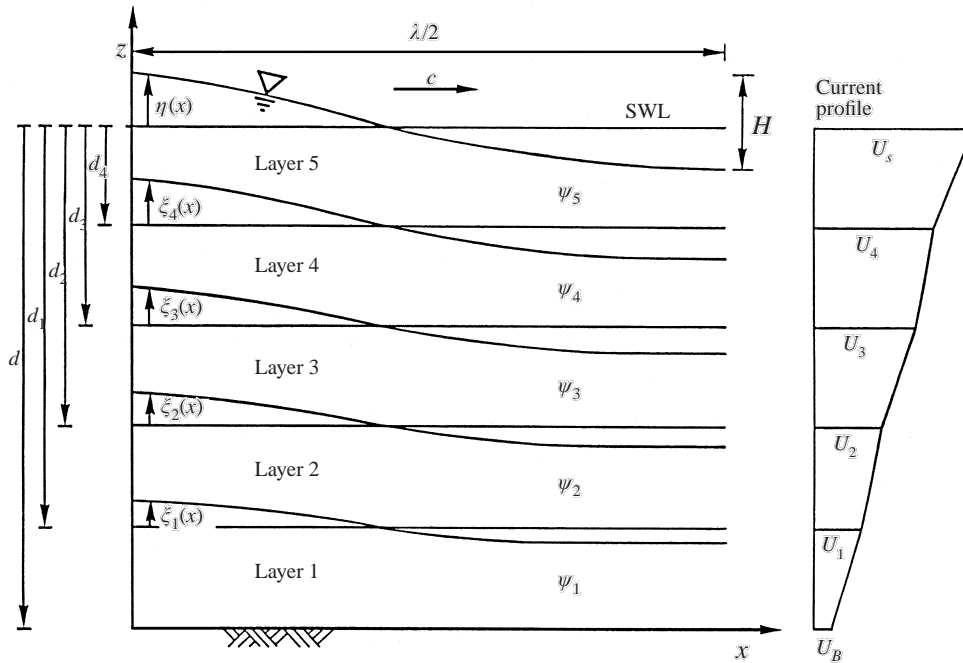


FIGURE 17. Coordinate arrangement and solution domain. (Note: Within this solution  $z$  is measured from the still water level upwards.)

train, the first two terms in (A 3) define the current profile, while the third defines the resulting wave motion. In addition to the  $(X_i, Y_i)$  unknowns, the required solution must solve for the wavenumber,  $k$ , the water-surface elevation,  $\eta$ , and the interfacial displacements,  $\xi_i$ , where  $i = 1, 2, 3, 4$  (figure 17). This gives a total of  $(2Nm + m + 1)$  unknowns, where  $m$  is the number of fluid layers, which is five in the present study. These unknowns are determined iteratively by minimizing the error in the following boundary conditions and equilibrium constraints.

A.1. External boundaries

If the bottom boundary is assumed to be both horizontal and impermeable, the vertical velocity must reduce to zero:

$$\frac{\partial \psi}{\partial z} = 0 \quad \text{on} \quad z = -d. \tag{A 4}$$

Assuming that  $z = \eta(x)$  defines the water-surface elevation, the kinematic free-surface boundary condition ensures that the water surface is a streamline:

$$\psi_5(x, z) = \psi_\eta = \text{constant} \quad \text{on} \quad z = \eta(x). \tag{A 5}$$

On  $z = \eta(x)$ , the dynamic free-surface boundary condition stipulates that the pressure is constant. Applying Bernoulli's equation yields

$$\eta(x) + \frac{1}{2g} \left[ \left( \frac{\partial \psi_5}{\partial x} \right)^2 + \left( \frac{\partial \psi_5}{\partial z} \right)^2 \right] = \text{constant} \quad \text{on} \quad z = \eta(x), \tag{A 6}$$

where  $g$  is the acceleration due to gravity.

## A.2. Interfacial boundary conditions

Within the proposed solution the interfacial boundaries must represent streamlines:

$$\psi(d_i + \xi_i) = \psi_{\xi_i} = \text{constant} \quad (\text{for } i = 1, 2, 3, 4). \quad (\text{A } 7)$$

Furthermore, the tangential velocities must be continuous across the boundaries:

$$\frac{\partial \psi_{i+1}}{\partial n} = \frac{\partial \psi_i}{\partial n} \quad \text{on } z = d_i + \xi_i(x) \quad \text{where } i = 1, 2, 3, 4, \quad (\text{A } 8)$$

where  $n$  defines a normal to the streamline.

## A.3. Equilibrium constraints

Since the present model is concerned with the equilibrium state associated with the combination of waves and currents, three further constraints may be imposed. First, the difference between the water-surface elevations arising at the wave crest and the wave trough must be equal to the specified wave height,  $H$ :

$$\eta(x = 0) - \eta(x = \frac{1}{2}\lambda) = H. \quad (\text{A } 9)$$

Secondly, there should be no mean change in the water depth:

$$\int_{x=0}^{x=\lambda/2} \eta(x) dx = 0, \quad (\text{A } 10)$$

and thirdly, there should be no mean displacement of the interfacial layers:

$$\int_{x=0}^{x=\lambda/2} \xi_i(x) dx = 0 \quad (\text{for } i = 1, 2, 3, 4). \quad (\text{A } 11)$$

The boundary conditions (A 4)–(A 8) and equilibrium constraints (A 9)–(A 11) are sufficient to define the  $(2Nm + m + 1)$  unknowns. The bottom boundary condition (A 4) may be satisfied exactly by setting

$$Y_i(n) = X_i(n) \tanh nkd, \quad (\text{A } 12)$$

where  $d$  is the total water depth; whilst (A 5) and (A 8) together with (A 3) allow  $\eta(x)$  and  $\xi_i(x)$  to be determined iteratively for given values of  $\psi_\eta$  and  $\psi_{\xi_i}$ , respectively. In the present study these calculations were undertaken using a simple Newton–Raphson formulation. The solution procedure is thus reduced to the determination of  $(2Nm - N + m + 1)$  unknowns, and develops accordingly:

(i) An initial estimate is made for  $\lambda_i, X_i(1), Y_i(1), \psi_\eta$  and  $\psi_{\xi_i}$  using a linear theory for waves on a uniform current ( $U = U_s$ ).

(ii) Equations (A 3), (A 5) and (A 7) are used to define  $\eta(x)$  and  $\xi_i(x)$  where  $i = 1, 2, 3, 4$ .

(iii) Assuming all the remaining unknowns are set to zero, an objective function is defined which expresses the sum of the mean square errors in (A 6), (A 8), (A 9), (A 10), and (A 11).

(iv) If this objective function is minimized with respect to the unknowns (and a number of Lagrange multipliers), sufficient equations are produced to define a new estimate for both the unknowns and the Lagrange multipliers.

(v) The new estimates for  $\psi_\eta$  and  $\psi_{\xi_i}$  are used to re-calculate the  $\eta(x)$  and  $\xi_i(x)$  (as (ii) above), and the iterative procedure continued until a converged solution is achieved.

Although this procedure is simplistic, the present calculations suggest that the computational demands are small, and that the procedure is robust in the sense

that a converged solution was achieved for all realistic (non-breaking) wave-current combinations. Using this approach typical calculations, involving a steep wave on a strongly sheared current, require the inclusion of eight harmonics and were undertaken on a standard PC with a 200 MHz Pentium processor. In the most nonlinear case, convergence was achieved after 100 iterations involving approximately five minutes of CPU time.

## REFERENCES

- BALDOCK, T. E., SWAN, C. & TAYLOR, P. 1996 A laboratory study of nonlinear surface waves on water. *Phil. Trans. R. Soc. Lond. A* **354**, 649–676.
- BREHERTON, F. P. & GARRETT, G. J. R. 1968 Wave trains in inhomogeneous moving media. *Proc. R. Soc. A* **302**, 529–554.
- BREVIK, I. 1980 Flume experiment on waves and currents II. Smooth bed. *Coastal Engng* **4**, 89–110.
- BREVIK, I. & AAS, B. 1980 Flume experiments on waves and currents I. Rippled bed. *Coastal Engng* **3**, 149–177.
- BREVIK, I. & SOLLIE, R. 1993 Energy flux and group velocity in currents of uniform vorticity. *Q. J. Mech. Appl. Maths* **46**, 117–130.
- BREVIK, I. & SOLLIE, R. 1997 Fluxes of mass, momentum and energy in currents of uniform vorticity. *Q. J. Mech. Appl. Maths* **50**, 1–16.
- BRINK-KJAER, O. 1976 Gravity waves on a current: the influence of vorticity, a sloping bed and dissipation. *Series paper 12*. Inst. Of Hydrodyn. & Hydraulic Engng, Tech. University of Denmark.
- CHAPLIN, J. R. 1980 Developments of stream function wave theory. *Coastal Engng* **3**, 179–205.
- CHAPLIN, J. R. 1990 The computation of nonlinear waves on a current of arbitrary non-uniform profile. OTH 90327, HMSO.
- CUMMINS, I. & SWAN, C. 1993 Nonlinear wave-current interactions. *Wave Kinematics and Environmental Forces. Soc. Underwater Tech.* **29**, 35–51.
- DALRYMPLE, R. A. 1973 Water wave models and wave forces with shear currents. *Tech. Rep. 20*. Coastal & Ocean Engng Lab., University of Florida.
- DALRYMPLE, R. A. 1974 Water waves on a bilinear shear current. In *Proc. 14th Conf. on Coastal Engng, Hamburg* (ed. B. L. Edge). ASCE, Vol. 1, pp. 626–641.
- DALRYMPLE, R. A. 1977 A numerical model for periodic finite amplitude waves on a rotational fluid. *J. Comput. Phys.* **24**, 29–44.
- DALRYMPLE, R. A. & HEIDEMAN, J. C. 1989 Nonlinear water waves on a vertically sheared current. *Proc. E & P Forum, Paris, Rep.* 3.12/156, pp. 69–92.
- DINGEMANS, M. W. 1997 *Water Wave Propagation over Uneven Bottoms. Part 1: Linear Wave Propagation*. The Advanced Series on Ocean Engineering, Vol. 13, pp. 237–239. World Scientific.
- DRAPER, L. 1957 Attenuation of sea waves with depth. *La Houille Blanche* **12**, 926–931.
- FENTON, J. D. 1985 A fifth-order Stokes theory for steady waves. *J. Waterway, Port, Coastal & Ocean Engng ASCE* **111**, 216–234.
- GROENEWEG, J. & KLOPMAN, G. 1998 Changes of the mean velocity profiles in the combined wave-current motion described in GLM formulation. *J. Fluid Mech.* **370**, 271–296.
- HEDGES, T. S. & LEE, B. W. 1992 The equivalent uniform current in wave-current computations. *Coastal Engng* **16**, 301–311.
- HSU, C. T., HSU, E. Y. & STREET, R. L. 1981 On the structure of turbulent flow over progressive water wave: theory and experiment in a transformed, wave following co-ordinate system. *J. Fluid Mech.* **105**, 87–117.
- JONSSON, I. G. 1990 Wave-current interactions. In *The Sea*, pp. 65–120. J. Wiley and Sons.
- JONSSON, I. G., BRINK-KJAER, O. & THOMAS, G. P. 1978 Wave action and set-down for waves on a shear current. *J. Fluid Mech.* **87**, 401–416.
- KEMP, P. H. & SIMONS, R. R. 1982 The interaction between waves and a turbulent current: waves propagating with the current. *J. Fluid Mech.* **116**, 227–250.
- KEMP, P. H. & SIMONS, R. R. 1983 The interaction between waves and a turbulent current: waves propagating against the current. *J. Fluid Mech.* **130**, 73–89.

- KIRBY, J. T. & CHEN, T. M. 1989 Surface waves on vertically sheared flows: Approximate dispersion relations. *J. Geophys. Res.* **94**, 1013–1027.
- KISHIDA, N. & SOBEY, R. J. 1988 Stokes theory for waves on a linear shear current. *J. Engng Mech.* **114**, 1317–1334.
- KLOPMAN, G. 1994 Vertical structure of flow due to waves and currents. *Progress Rep. Delft Hydraulics* H 840.32, Part 2.
- KOOLE, R. & SWAN, C. 1994 Measurements of a 2-D non-buoyant jet in a wave environment. *Coastal Engng* **24**, 151–169.
- LONGUET-HIGGINS, M. S. 1953 Mass transport in water waves. *Phil. Trans. R. Soc. Lond. A* **245**, 535–581.
- LONGUET-HIGGINS, M. S. & STEWART, R. W. 1960 Changes in the form of short gravity waves on long waves and tidal currents. *J. Fluid Mech.* **8**, 565–583.
- PEREGRINE, D. H. 1976 Interaction of water waves and currents. *Adv. Appl. Mech.* **16**, 9–117.
- SIMMEN, J. A. & SAFFMAN, P. G. 1985 Steady deep water waves on a linear shear current. *Stud. Appl. Maths* **73**, 35–57.
- SKOP, R. A. 1987 An approach to the analysis of the interaction of surface waves with depth-varying current fields. *App. Math. Modelling* **11**, 432–437.
- SKYNER, D. J. & EASSON, W. J. 1992 The effect of sheared currents on wave kinematics and surface parameters. In *Proc. 23rd Intl Conf. on Coastal Engng, Venice, Italy* (ed. B. L. Edge). ASCE, Vol. 1, pp. 618–629.
- SKYNER, D. J. & EASSON, W. J. 1998 Wave kinematics and surface parameters of steep waves travelling on sheared currents. *J. Waterway, Port, Coastal, Ocean Engng ASCE* **124**, 1–7.
- SOBEY, R. J., GOODWIN, P., THIEKE, R. J. & WESTBERG, R. J. 1987 Application of Stokes, Cnoidal and Fourier wave theories. *J. Waterway, Port, Coastal, Ocean Engng ASCE* **113**, 565–587.
- STEWART, R. H. & JOY, J. W. 1974 HF radio measurements of surface currents. *Deep-Sea Res.* **21**, 1039–1049.
- SWAN, C. 1990 An experimental study of waves on a strongly sheared current profile. In *Proc. 22nd Intl Conf. on Coastal Engng, Delft* (ed. B. L. Edge). ASCE, Vol. 1, pp. 489–502.
- SWAN, C. & JAMES, R. L. 2000 A simple analytical model for surface water waves on a depth-varying current. Submitted to *Appl. Ocean Res.*
- SWAN, C. & SLEATH, J. F. A. 1990 A second approximation to the time-mean Lagrangian drift beneath a series of progressive gravity waves. *Ocean Engng* **17**, 65–79.
- TELES DA SILVA, A. F. & PEREGRINE, D. H. 1988 Steep, steady surface waves on water of finite depth with constant vorticity. *J. Fluid Mech.* **195**, 281–302.
- THOMAS, G. P. 1981 Wave-current interactions: an experimental and numerical study. Part 1. Linear waves. *J. Fluid Mech.* **110**, 457–474.
- THOMAS, G. P. 1990 Wave-current interactions: an experimental and numerical study. Part 2. Nonlinear waves. *J. Fluid Mech.* **216**, 505–536.
- THOMAS, G. P. & KLOPMAN, G. 1997 Wave-current interactions in the nearshore region. In *Gravity Waves in Water of Finite Depth* (ed. J. N. Hunt), pp. 215–319. Computational Mechanics Publications.
- TSAO, S. 1959 Behaviour of surface waves on a linearly varying flow. *Tr. Mosk. Fiz.-Tekh. Inst. Issled. Mekh. Prikl. Mat.* **3**, 66–84.
- WHITE, B. S. 1999 Wave action on currents with vorticity. *J. Fluid Mech.* **386**, 329–344.